

DISTANT AND LOCAL TSUNAMIS IN  
COASTAL REGIONS

PB81-211047

by

Jiin-Jen Lee

Associate Professor of Civil Engineering  
(Principal Investigator)

Other Contributors:

S.T. Kim, Research Associate of Civil Engineering  
R.M. Ayer, Research Assistant of Civil Engineering  
J.J. Chang, Research Assistant of Civil Engineering

Final Report .  
to  
National Science Foundation  
(Grant No. ENV 77-01599)

Department of Civil Engineering  
University of Southern California  
Los Angeles, Calif. 90007

December 1980

**Any opinions, findings, conclusions  
or recommendations expressed in this  
publication are those of the author(s)  
and do not necessarily reflect the views  
of the National Science Foundation.**

**INFORMATION RESOURCES  
NATIONAL SCIENCE FOUNDATION**



REPORT DOCUMENTATION PAGE		1. REPORT NO. NSF/RA-800511	2.	3. Recipient's Accession No. <b>PD81 211047</b>
4. Title and Subtitle Distant and Local Tsunamis in Coastal Region(s), Final Report			5. Report Date December 1980	
7. Author(s) J.-J. Lee, S. T. Kim, R. M. Ayer, J. J. Chang			6.	
9. Performing Organization Name and Address University of Southern California Department of Civil Engineering Los Angeles, CA 90007			8. Performing Organization Rept. No.	
12. Sponsoring Organization Name and Address Engineering and Applied Science (EAS) National Science Foundation 1800 G Street, N.W. Washington, DC 20550			10. Project/Task/Work Unit No.	
			11. Contract(C) or Grant(G) No. (C) (G) ENV7701599	
15. Supplementary Notes Submitted by: Communications Program (OPRM) National Science Foundation Washington, D.C. 20550			13. Type of Report & Period Covered Final	
16. Abstract (Limit: 200 words)  The generation and propagation of tsunamis occurring in coastal regions between November 1977 and April 1980 are analyzed. Focus is on three subject areas: (1) the generation of water waves by three-dimensional bed motion; (2) a viscous model for nonlinear dispersive waves; and (3) the propagation of linear periodic waves over submarine trenches. The experimental design for each phase is presented including its problem formulation and both theoretical and numerical analyses. Results of the first part show that three-dimensional water surface profiles deviate significantly from two-dimensional water profiles. The second phase indicates that the effect of nonlinearity, dispersion, and dissipation are equally important in defining the behavior of wave propagation. The third part demonstrates that for a particular flow configuration, an infinite number of discrete wave frequencies exist at which waves are completely transmitted. Three-dimensional drawings and graphs illustrate the discussions.			14.	
17. Document Analysis a. Descriptors				
Tsunamis		Wave generators	Nonlinear systems	
Wave propagation		Seismic waves	Numerical analysis	
Wave dispersion		Simulation	Coasts	
b. Identifiers/Open-Ended Terms				
REPRODUCED BY <b>NATIONAL TECHNICAL          INFORMATION SERVICE</b> U.S. DEPARTMENT OF COMMERCE SPRINGFIELD, VA 22161				
c. COSATI Field/Group				
18. Availability Statement			19. Security Class (This Report)	21. No. of Pages
			20. Security Class (This Page)	22. Price



## TABLE OF CONTENTS

Chapter 1	General Overview and Research Summary.	1
Chapter 2	Generation of Water Waves by Three Dimensional Bed Motion.	7
Chapter 3	A Viscous Model for Non-linear Dispersive Waves.	29
Chapter 4	Wave Propagation Over Submarine Over Submarine Trench.	60

### Publications

Appendix I	An Inclined Plate Generator.	89
Appendix II	Waves Generated by an Impulsive Bed Motion of Finite Size.	96
Appendix III	Water Waves Generated by an Impulsive Bed Upthrust of a Rectangular Block.	107
Appendix IV	Wave Propagation Over Rectangular Trench.	114
Appendix V	Interaction of Waves with Submarine Trenches.	130
Appendix VI	Water Waves Generated by Three Dimensional Bed Motion.	142



## Chapter 1 General Overview and Research Summary

This report contains research findings of a research project entitled "Distant and Local Tsunamis in Coastal Regions" during the period November 15, 1977 to April 30, 1980. The research was supported by the Earthquake Hazards Mitigation Program, National Science Foundation.

Several aspects of the generation and propagation of tsunamis have been investigated. Results have been obtained; they will be presented herein. "Tsunamis" are water waves generated through tectonic displacements associated with submarine earthquakes, volcanic eruptions and/or indirectly by submarine slumps and shoreline landslides. These waves have also been called "tidal waves" although the waves are not generated by tides. The Japanese word "tsunamis" literally means "harbor waves." This is a very descriptive term because the major damages caused by this type of wave usually occurs in bays and harbors near the coastal zone.

The wave length of a tsunami generated in the deep ocean is usually very long, however, the amplitude of the wave is relatively small compared with wave length. In this deep ocean region the water surface is so small that they cannot be easily detected. The propagation speeds of these waves in the deep ocean region are quite large and approximately equal to  $\sqrt{gh}$  (where  $g$  is the gravitational acceleration and  $h$  is the water depth). As these waves approach a coastal region, due to the decrease in water depth, the propagation speeds of these waves are reduced. Therefore, the wave amplitude will be increased in the region of shallow water depth. In addition, the local topography of a particular region could induce resonant oscillations of these waves thereby significantly amplifying the wave amplitude. Such large oscillating waves could present major

hazards to life and property in the coastal zone especially if the region is heavily populated.

Research results on three areas of investigation related to generation and propagation of tsunamis are presented in Chapters 2, 3, and 4. A brief summary of the major results will be provided below.

Chapter 2 presents the results of a theoretical and numerical study on the generation of water waves due to three-dimensional bed motion. Prior to the study, waves generated due to a two-dimensional bed motion have been obtained both theoretically and experimentally. However, experience has shown that the natural bed motion has always been finite in size, the two-dimensional assumption cannot be considered as a realistic situation. Therefore, it is thought that consideration of three-dimensional bed motion would produce a more realistic picture of the nature of tsunami wave generation. This has been accomplished. An analytical model has been developed and the theoretical results have been obtained. They help define the limitation of the two-dimensional results and demonstrates the complicated wave pattern which is generated. The work in Chapter 2 is performed by J. J. Lee and J. J. Chang. A summary of the work is provided as follows:

A theoretical and digital simulation on waves generated by an impulsive bed upthrust of a rectangular block with various ratios of length/width is presented. The two-dimensional Fast Fourier Transform (FFT) algorithm is used to obtain the water surface profile near the generation region. The three-dimensional pictures were constructed from an array of 256 X 256 pixel by using Image Processing. Comparison of the present three-dimensional results, with previously published

two-dimensional results, indicates that for large length/width ratios, the water surface profile is quite similar at certain locations for a small time after the impulsive bed motion is completed. Generally, the water surface profiles deviate significantly from the two-dimensional results.

Chapter 3 presents the results of a viscous model for the propagation of non-linear and dispersive waves. The primary motivation for this research effort was to include the effect of viscous dissipation on the propagation of nonlinear, dispersive waves. The result of the present study showed that, in the laboratory scales, the effect of nonlinearity, dispersion and dissipation are equally important in defining the behavior of wave propagation. Although it can be argued that for the prototype scale, the effort of viscous dissipation would be smaller in the propagation phase of the tsunami problem. This portion of the study is performed by J. J. Lee and S. T. Kim. A summary of the work is provided below:

A modified Korteweg-de Vries (KdV) equation has been derived to represent approximately the propagation of non-linear, dispersive long waves including dissipation effects. The equation is found by including the effect of the laminar boundary layer at the bottom. Numerical solutions of the derived equation under various initial conditions have also been obtained. Good agreement has been found when comparing the numerical results with the experimental profiles of Hammack (1973) and Hammack & Segur (1974). For a solitary wave propagating in a shallow water of constant depth, the present results also show good agreement with the prior published theories.

Chapter 4 presents the results of a theoretical and numerical study on the propagation of linear periodic waves over submarine trenches. For this aspect of the research, effort is directed to developing an analytical method for analyzing the wave propagation over submarine trenches where a sharp discontinuity in the water depth occurs. The result could be applied to two practical situations:

- (1) For waves in the deep ocean region, the effect of the deep submarine trenches on long tsunami waves can be analyzed by the method developed herein.
- (2) For waves in the coastal region, especially for harbor regions, the effect of navigation channel on the normally incident waves can be assessed.

This portion of the work is performed by J. J. Lee and R. M. Ayer. A summary of the work is provided below:

An analysis is presented for the propagation of water waves past a rectangular submarine trench. Two-dimensional, linearized potential flow is assumed. The fluid domain is divided into two regions along the mouth of the trench. Solutions in each region are expressed in terms of the unknown normal derivative of the potential function along this common boundary with the final solution obtained by matching. Reflection and transmission coefficients are found for various submarine geometries. The result shows that for a particular flow configuration, there exists an infinite number of discrete wave frequencies at which waves are completely transmitted. The validity of the solution in the infinite constant water depth region is shown by

comparing with the results using boundary integral method for given velocity distributions along the mouth of the trench. The accuracy of the matching procedure is also demonstrated through the results of the boundary integral technique. In addition, laboratory experiments were performed and are compared with the theory for two of the cases considered.

In the Appendix of this report, the reprints or preprints of the published work are provided. They contain the following publications:

1. "An Inclined-Plate Wave Generator" by F. Raichlen and J. J. Lee, Chapter 21 of the Proceedings of 16th International Coastal Engineering Conference, Hamburg, Germany, 1978, pp. 388-399.
2. "Wave Generated by an Impulsive Bed Motion of Finite Size" by J. J. Lee and J. J. Chang, Proceedings of the International Conference on Water Resources Development, May 12-14, 1980, Taipei, Taiwan, pp. 759-768.
3. "Water Waves Generated by An Impulsive Bed Upthrust of a Rectangular Block" by J. J. Lee and J. J. Chang, Applied Ocean Research, Vol. 2, No. 4, Oct. 1980, pp. 165-170.
4. "Interactions of Waves With Submarine Trenches" by J. J. Lee, R. M. Ayer and W. L. Chiang, Proceedings of the 17th International Coastal Engineering Conference, Sydney, Australia, March 1980.
5. "Wave Propagation Over Rectangular Trench" by J. J. Lee and R. M. Ayer, to appear in the Journal of Fluid Mechanics, 1981 (accepted Dec. 1980).

6. "Water Waves Generated by Three Dimensional Bed Motion" by J. J. Chang and J. J. Lee, paper to be presented at the International Tsunami Symposium, May 25-29, 1981, Japan.

## 1. Introduction

Waves generated by submarine earthquakes, commonly known as tsunamis, have been of interest to ocean and coastal engineers. In many instances, such waves have caused significant damage to the coastal region. Estimation of the tsunami wave form is essential for the prediction of the wave profile in the propagation phase and the final wave form when the wave arrives in the coastal region.

Most of the theoretical models of tsunami generation have been based on linearized theory in either a two- or three-dimensional fluid domain of uniform depth. Based on the linear theory, the fundamental solution of the wave forms can be obtained by multiple Fourier Transforms such as that used by Driessche and Braddock (1972) and Hammack (1972, 1973) or by the Green's function method used by Kajiura (1963, 1970).

The complexity of the integral solution has discouraged many authors from obtaining detailed wave behavior near the generation region even in the case of a simple bed deformation model. Instead, many authors have been using asymptotic methods to evaluate the integrals. Consequently, only the far-field wave behavior can be examined.

For three-dimensional wave generation models, the computational effort needed to evaluate the integrals by means of conventional numerical integration schemes have been quite laborious. To overcome this difficulty, the modern digital simulation technique can be used to significantly improve the computational efficiency.

This paper presents results of a theoretical and digital simu-

lation study on waves generated by an impulsive bed motion. For mathematical simplicity, the extent of the bottom disturbance is assumed to be of rectangular shape although an elliptic shape might be a better tsunami generation model (See Horikawa, 1978). The fundamental solution for the wave amplitude is expressed in terms of multiple integrals which are evaluated by utilizing the two-dimensional Fast Fourier Transform (FFT) algorithm. The three-dimensional pictures (based on 256 X 256 samples) showing aspects of wave decay everywhere in the fluid domain at a specified time are obtained by the Image Processing technique.

## 2. Problem Formulation

Let  $(x,y,z)$  constitute a Cartesian coordinate system with  $z = 0$  as the undisturbed water surface as shown in the definition sketch in Figure 1. Initially, the fluid is at rest with the free surface and solid boundary defined by  $z = 0$  and  $z = -h$ , respectively ( $h$  is a constant). For  $t > 0$ , the solid boundary is permitted to move as prescribed by  $\xi(x,y;t)$ . The resulting deformation of the free surface is to be determined as  $z = \eta(x,y;t)$ . Assuming irrotational flow and an inviscid fluid, the fluid kinematics can be expressed in terms of a velocity potential  $\phi(x,y,z;t)$ . The differential equation and the linearized boundary conditions that  $\phi$  must satisfy can be listed as follows:

$$\nabla^2 \phi = 0 \quad 0 < t < \infty, -\infty < x,y < \infty, -h < z < 0 \quad (1)$$

$$\phi_{tt} + g\phi_z = 0 \quad z = 0 \quad (2)$$

$$\phi_z = \xi_t(x,y;t) \quad z = -h \quad (3)$$

In these equations, the subscripts denote partial derivatives and  $g$  denotes the gravitational acceleration.

The linearized relation between the water surface displacement  $\eta$  and the velocity potential  $\phi$  is:

$$\eta(x,y;t) = -\frac{1}{g} \phi_t(x,y,0;t) \quad (4)$$

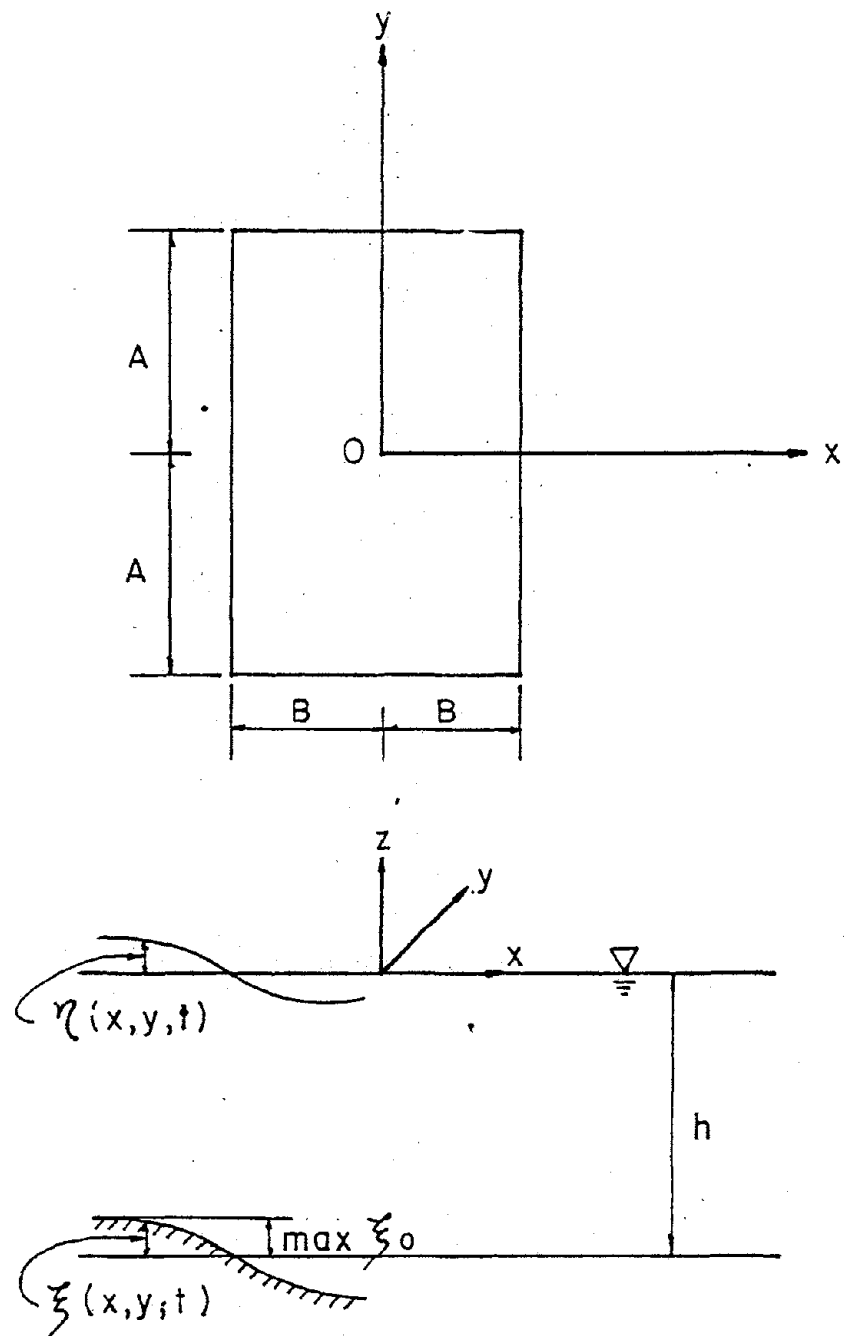


FIG. 1 DEFINITION SKETCH OF FLUID DOMAIN AND CO-ORDINATE SYSTEM

The solution for  $\phi$  (and hence,  $\eta$ ) is obtained by using the Fourier transform for the spatial variables  $x$ ,  $y$  and the Laplace transform for the time variable  $t$  defined by

$$\hat{f}(K_1, K_2, s) = \int_0^\infty e^{-st} \int_{-\infty}^\infty e^{iK_2 y} \int_{-\infty}^\infty e^{iK_1 x} f(x, y; t) dx dy dt \quad (5)$$

By applying the transformation of Equation (5) to the governing equation and boundary conditions with the subsequent inversion, one obtains the water surface elevation as:

$$\eta(x, y, t) = \frac{1}{(2\pi)^2} \int_{-\infty}^\infty \int_{-\infty}^\infty \left( \frac{1}{2\pi i} \int_{Br} \frac{s^2 e^{-iK_1 x} e^{-iK_2 y} e^{st} \hat{\xi}(K_1, K_2, s)}{(s^2 + \omega^2) \cosh \sqrt{K_1^2 + K_2^2} h} ds \right) dK_1 dK_2 \quad (6)$$

where  $\int_{Br} \equiv \lim_{\Gamma \rightarrow \infty} \int_{\mu+i\Gamma}^{\mu+i\Gamma}$  is the Bromwich contour,  $\omega$  is the circular frequency and  $\mu$  is a positive constant.

In order to obtain the specific wave profile as defined in Equation (6), one must specify the bed deformation history  $\xi(x, y; t)$ . The bed deformation is assumed to be a rectangular block upthrust with exponential variation in time:

$$\xi(x, y, t) = \xi_0 (1 - e^{-\alpha t}) H(B^2 - x^2) H(A^2 - y^2) \text{ for } t \geq 0 \quad (7)$$

where  $\xi_0$  is the maximum amplitude of the vertical displacement,  $\alpha$  is the time constant defined as  $1.11/t_c$ , and  $t_c$  is the characteristic time defined by  $\xi/\xi_0 = 2/3$  at  $t = t_c$ . The Heavyside step function is defined as:

$$H(B^2-x^2) = \begin{cases} 1, & B^2-x^2>0 \\ 0, & B^2-x^2<0 \end{cases} \quad \text{and} \quad H(A^2-y^2) = \begin{cases} 1, & A^2-y^2>0 \\ 0, & A^2-y^2<0 \end{cases}$$

The transformation of Equation (7) yields:

$$\hat{\xi}(K_1, K_2, s) = 4\xi_0 \frac{\sin K_1 B}{K_1} \cdot \frac{\sin K_2 A}{K_2} \left[ \frac{\alpha}{s(s+\alpha)} \right] \quad (8)$$

Substituting Equation (8) into Equation (6) and solving for the surface elevation yields:

$$\eta(x, y, t) = -\frac{\xi_0}{\pi^2} \int_{-\infty}^{\infty} \int_{-\infty}^{\infty} e^{iK_1 x} e^{iK_2 y} \frac{\sin K_1 B}{K_1} \frac{\sin K_2 A}{K_2} \frac{1}{\cosh \sqrt{K_1^2 + K_2^2} h} \left[ \frac{\alpha^2}{\alpha^2 + \omega^2} (e^{-\alpha t} - \cos \omega t - \frac{\omega}{\alpha} \sin \omega t) \right] dK_1 dK_2 \quad (9)$$

where

$$\omega^2 = g \sqrt{K_1^2 + K_2^2} \tanh \sqrt{K_1^2 + K_2^2} h$$

Equation (9) contains poles at  $K_1 = 0$  and/or  $K_2 = 0$ . These singularities can be treated easily by L'Hospital's rule. The reader is reminded that Equation (9) can be reduced to the two-dimensional solution given by Hammack (1973) by integration with respect to  $K_2$  as  $A \rightarrow \infty$ . (This is easily accomplished by changing the variable of integration to  $(K_2 \cdot A)/A$  and evaluate the integral as  $A \rightarrow \infty$ ). Introducing  $K_1 = 2\pi k_1$  and  $K_2 = 2\pi k_2$ , Equation (9) can be rewritten as

$$\eta(x,y,t) = -4\xi_0 \int_{-\infty}^{\infty} \int_{-\infty}^{\infty} e^{i2\pi k_1 x} e^{i2\pi k_2 y} f(k_1, k_2) dk_1 dk_2 \quad (10)$$

where  $f(k_1, k_2)$  is a symmetric function defined by

$$f(k_1, k_2) = \frac{\sin 2\pi k_1 B}{2\pi k_1} \frac{\sin 2\pi k_2 A}{2\pi k_2} \frac{1}{\cosh \sqrt{(2\pi k_1)^2 + (2\pi k_2)^2} h} \left[ \frac{\alpha^2}{\alpha^2 + \omega^2} (e^{-\alpha t} - \cos \omega t - \frac{\omega}{\alpha} \sin \omega t) \right]$$

and

$$\omega^2 = g \sqrt{(2\pi k_1)^2 + (2\pi k_2)^2} \tanh \sqrt{(2\pi k_1)^2 + (2\pi k_2)^2} h.$$

It should be recognized that Equation 10 is a two-dimensional Fourier Transform of  $f(k_1, k_2)$  and can be computed by using the Fast Fourier Transform (FFT).

### 3. Numerical Implementation

Suppose that  $f(k_1, k_2)$  is defined in the interval of  $-T/2 < k_1, k_2 < T/2$  and is zero for  $|k_1|, |k_2| > T/2$ . Equation (10) can then be written as:

$$\eta(x, y, t) = -4\varepsilon_0 \int_{-T}^T \int_{-T}^T f(k_1, k_2) e^{i2\pi k_1 x} e^{i2\pi k_2 y} dk_1 dk_2 \quad (11)$$

It should be noted that the conventional procedure of computing  $\eta(x, y, t)$  in Equation (11) by fixing a set of  $(x, y; t)$  is quite inefficient. For our purpose, a more advantageous procedure is to fix a time  $t = t_i$  and evaluate Equation (11) for all possible  $x$  and  $y$  by recognizing Equation (11) as a double Fourier Transform of  $f(k_1, k_2; t_i)$ .

The integral in Equation (11) can be approximated by a Reimann sum to be presented as follows:

Choosing  $\varepsilon > 0$ , then there exists  $\delta > 0$  such that

$$\left| \eta(x, y, t) - \sum_{n_1=-N_1/2+1}^{N_1/2} \sum_{n_2=-N_2/2+1}^{N_2/2} (k_{n_1+1} - k_{n_1})(k_{n_2+1} - k_{n_2}) f(k'_{n_1}, k'_{n_2}) e^{i2\pi k'_{n_1} x} e^{i2\pi k'_{n_2} y} \right| < \varepsilon$$

provided that

$$k_{n_i} \leq k'_{n_i} < k_{n_{i+1}} \quad \text{and} \quad k_{n_{i+1}} - k_{n_i} < \delta$$

for all  $(n_i = -N_i/2 + 1, -N_i/2 + 2, \dots, N_i/2)$  for  $i = 1, 2$ . Where  $N_1$  and  $N_2$  are the number of discrete points which correspond to the  $x$  and  $y$  axis, respectively.

It is convenient to choose the intervals  $(k_{n_i}, k_{n_i+1})$  to be of constant length,  $\Delta k_i$ , for  $i = 1, 2$ . Thus Equation (11) can be approximated as:

$$\eta(x, y, t) = -4\xi_0 \sum_{n_1=-N_1/2+1}^{N_1/2} \sum_{n_2=-N_2/2+1}^{N_2/2} f(n_1 \Delta k_1; n_2 \Delta k_2) e^{i2\pi x n_1 \Delta k_1} e^{i2\pi y n_2 \Delta k_2} \cdot \Delta k_1 \Delta k_2 \quad (12)$$

where  $\Delta k_i = 2T/N_i$  for  $i = 1, 2$ . This definition of  $\Delta k_i$  implies that  $\Delta x = \Delta y = 1/(2T)$ . By introducing  $x = k_1 \cdot \Delta x$ ,  $y = k_2 \cdot \Delta y$ ,  $\omega_1 = e^{2\pi i/N_1}$  and  $\omega_2 = e^{2\pi i/N_2}$  we can rewrite Equation (12) as follows:

$$\eta(k_1, k_2; t) = -4\xi_0 \Delta k_1 \Delta k_2 \sum_{n_1=-N_1/2+1}^{N_1/2} \sum_{n_2=-N_2/2+1}^{N_2/2} f(n_1, n_2) \omega_1^{k_1 n_1} \omega_2^{k_2 n_2} \quad (13)$$

for  $-N_1/2 + 1 \leq k_1 \leq N_1/2$ ,  $-N_2/2 + 1 \leq k_2 \leq N_2/2$

where

$$f(n_1, n_2) = \frac{\sin 2\pi n_1 \Delta k_1 B}{2\pi n_1 \Delta k_1} \cdot \frac{\sin 2\pi n_2 \Delta k_2 A}{2\pi n_2 \Delta k_2} \cdot \frac{1}{\cosh \sqrt{(2\pi n_1 \Delta k_1)^2 + (2\pi n_2 \Delta k_2)^2} h} \cdot \left[ \frac{\alpha^2}{\alpha^2 + \omega^2} (e^{-st} - \cos \omega t - \frac{\omega}{\alpha} \sin \omega t) \right]$$

and

$$\omega^2 = g \sqrt{(2\pi n_1 \Delta k_1)^2 + (2\pi n_2 \Delta k_2)^2} \tanh \sqrt{(2\pi n_1 \Delta k_1)^2 + (2\pi n_2 \Delta k_2)^2} h$$

It should be noted that  $\omega_1$  and  $\omega_2$  introduced in Equation (13) is a  $N_1$ -th and  $N_2$ -th root of unity in the complex number field, respectively.

Equation (13) is a two-dimensional Discrete Fourier Transform and can be evaluated by the following two stages of computation:

$$\begin{aligned} \text{Stage 1: } \eta'(n_1, k_1, t) &= C_1 \sum_{n_2=-N_2/2+1}^{N_2/2} f(n_1, n_2) \omega_2^{k_2 n_2}; \\ \text{for } -\frac{N_2}{2} + 1 &\leq k_2 \leq \frac{N_2}{2}, \text{ where } C_1 = -4\xi_0 \Delta k_1 \Delta k_2. \end{aligned} \quad (14-A)$$

$$\begin{aligned} \text{Stage 2: } \eta(k_1, k_2, t) &= \sum_{n_1=-N_1/2+1}^{N_1/2} \eta'(n_1, k_2, t) \omega_1^{k_1 n_1}; \\ \text{for } -\frac{N_2}{2} + 1 &\leq k_1 \leq \frac{N_2}{2} \end{aligned} \quad (14-B)$$

We observe that Stage 1 and Stage 2 are two one-dimensional Discrete Fourier Transforms of  $f(n_1, n_2)$ . If we let  $N_1 = N_2 = 2^m$  where  $m$  is an integer, then the FFT algorithm can be used to compute  $\eta'(n_1, k_2, t)$  and  $\eta(k_1, k_2, t)$  (See Oppenheim and Schaffer (1975)). The number of real multiplications and additions needed to compute Equations (14-A) and (14-B) is  $4N^2 \log_2 N$  and  $6N^2 \log_2 N$ , respectively.

An array of 256 X 256 points was used to compute Equations (14-A) and (14-B) ( $N_1 = N_2 = 256$ ). To avoid the spurious short-period oscillations,  $k$  should be kept small. However, a small  $\Delta k$  implies that the region of computation is also correspondingly limited. All numerical results presented in this paper are obtained for  $\Delta k = 0.03$ . This value was arrived at through a series of numerical experiments.

#### 4. Presentation and Discussion of Results

Numerical results obtained from Equations (13) and (14) for an impulsive bed upthrust of a rectangular block with various aspect ratios ( $A/B$ ) have been obtained. The two-dimensional case of the same bed motion characteristics, i.e., for  $A \rightarrow \infty$ , has been studied by Hammack (1973) both theoretically and experimentally in which it was found that the theoretical results agreed well with the experimental results.

As the three-dimensional experimental results are not available, it is advantageous for us to study such a case with various aspect ratios. It is reasonable to expect that for large values of  $A/B$ , our results should approach that reported by Hammack (1973). The water surface profiles as a function of the dimensionless time parameter ( $t\sqrt{g/h}$ ) at three different locations are shown in Figure 2. The dimensionless parameters for this case are:  $t_c\sqrt{gh}/B = 0.069$ ,  $B/h = 12.2$  ( $B = 2.0$  ft.),  $\xi_0/h = 0.2$ . The time history of bed motion is an exponential form as seen in Equation (7) with a characteristic time parameter,  $\alpha = 18.46$ . In Figure 2, the time history of the water surface profiles for  $A/B = 10$ , 5, and 2 are shown for three locations ( $x = y = 0$ ), ( $x = B$ ,  $y = 0$ ), and ( $x = 0$ ,  $y = A$ ). It is seen that the curves for  $A/B = 10$ , 5 and 2 are very close to that of Hammack's at the first two locations. For  $A/B = 2$ , the three-dimensional effect becomes quite significant for  $t\sqrt{g/h} > 20$  as evidenced in Figure 2. Based on the physical dimensions given, the time associated with  $t\sqrt{g/h} = 20$  is  $t = 1.426$  sec. This is smaller than the time required for disturbance to propagate from the edge of the rectangular

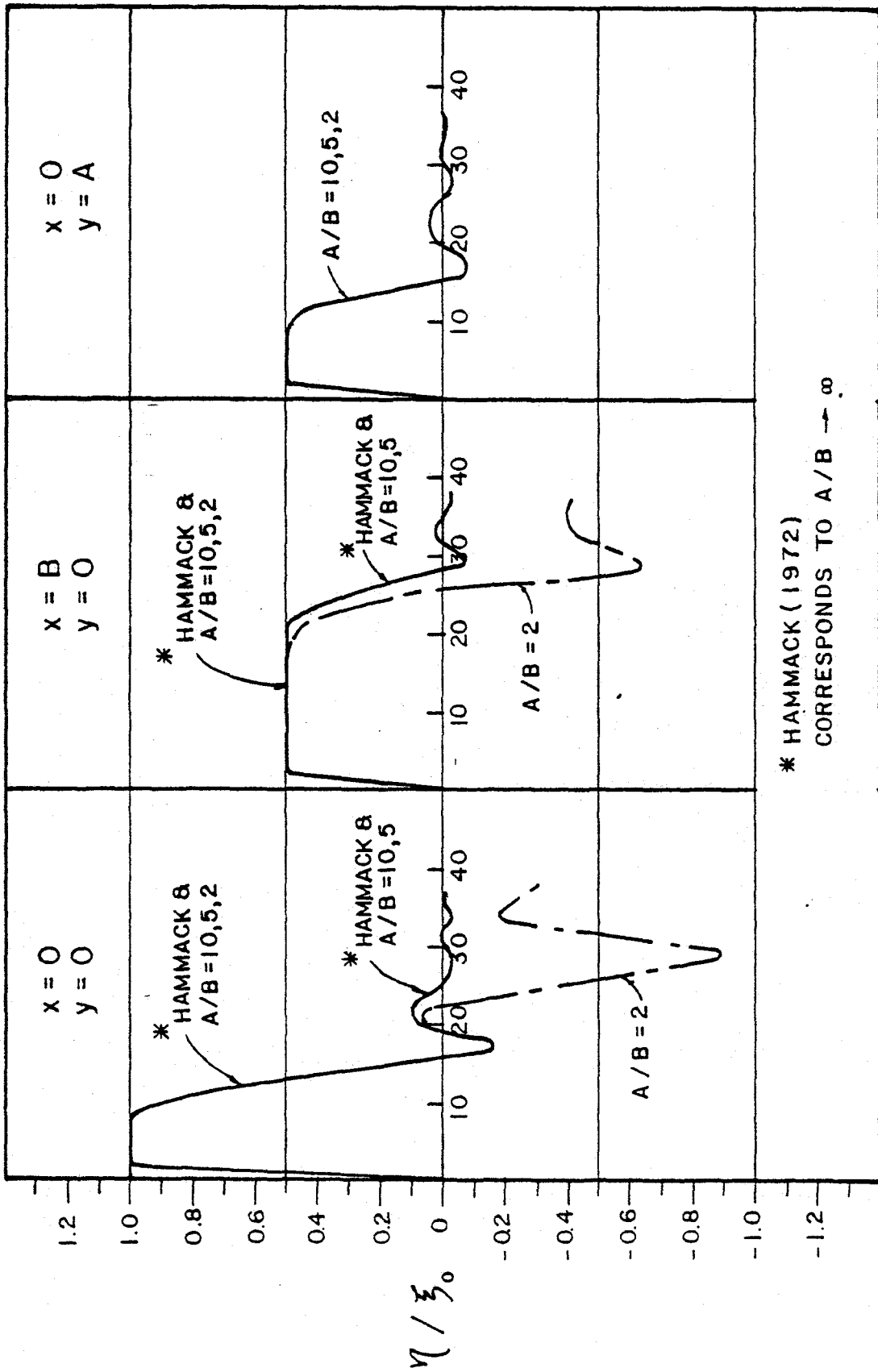


FIG. 2 WATER SURFACE PROFILES FOR DIFFERENT LENGTH / WIDTH RATIO AT  $x=0, y=0$ ;  $x=B, y=0$ ; AND  $x=0, y=A$

block ( $y = A$ ) to the center ( $y = 0$ ) if one assumes the propagation speed to be  $\sqrt{gh} = 2.3$  fps. (This latter time is computed to be 1.734 sec.). It should be noted that the early arrival of end effects (with relation to the propagation speed of  $\sqrt{gh}$ ) as  $A$  is reduced suggests that some of the Fourier components composing the corner region of the initial disturbance have phase shifts so that they have distances less than  $A$  to travel before reaching the location  $(B,0)$ . The phase shifts will be relatively smaller as  $A$  is increased. The third graph shows the water surface profile as a function of time at the edge of the major axis ( $x = 0, y = A$ ). This provides another view of the three-dimensional effect. We note that for the two-dimensional case, the water surface profile at  $x = 0, y = A$ , would be the same as that shown for  $x = 0, y = 0$ . However, for a finite ratio of  $A/B$ , the edge effect of the generation region is being felt instantly after the impulsive bed motion is produced.

The water surface profiles as a function of time at other locations away from the region of rectangular block are shown in Figure 3 for  $A/B = 5$  and  $A/B = 2$ . The three locations chosen are all along the minor axis ( $y = 0$ ) and at  $x = 1.5B, 2.0B$ , and  $2.5B$ . The three-dimensional effect is also quite obvious; for  $A/B = 2$ , a negative wave occurs at a smaller value of  $t\sqrt{g/h}$ .

It is interesting to see some three-dimensional pictures of the water surface profile. A series of three-dimensional pictures for the case  $A/B = 2$  is presented in Figure 4 and Figure 5. These three-dimensional pictures were constructed from 256 X 256 samples using Image Processing (Readers interested in Image Processing are referred to Andrews (1970)).

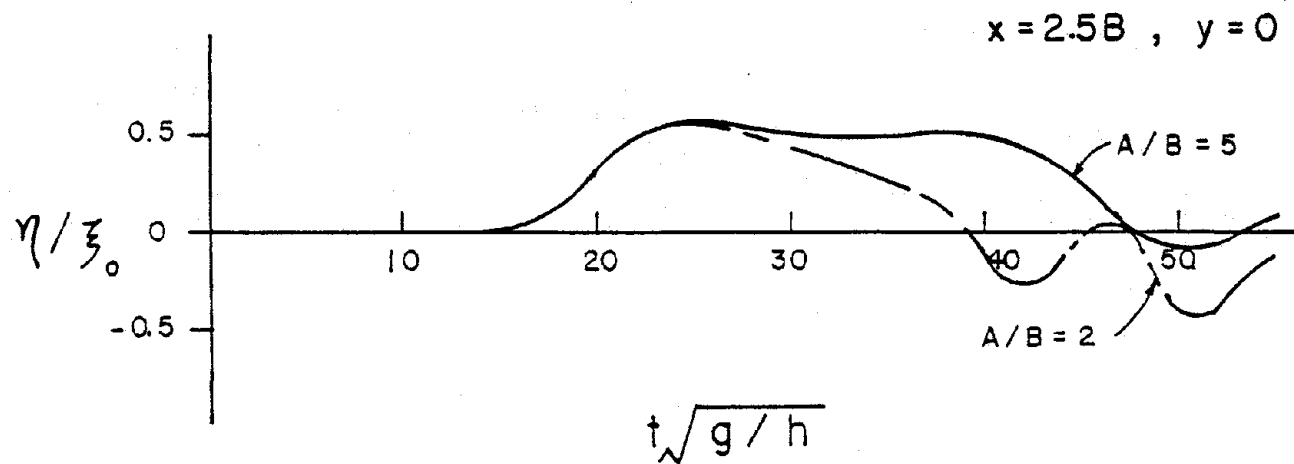
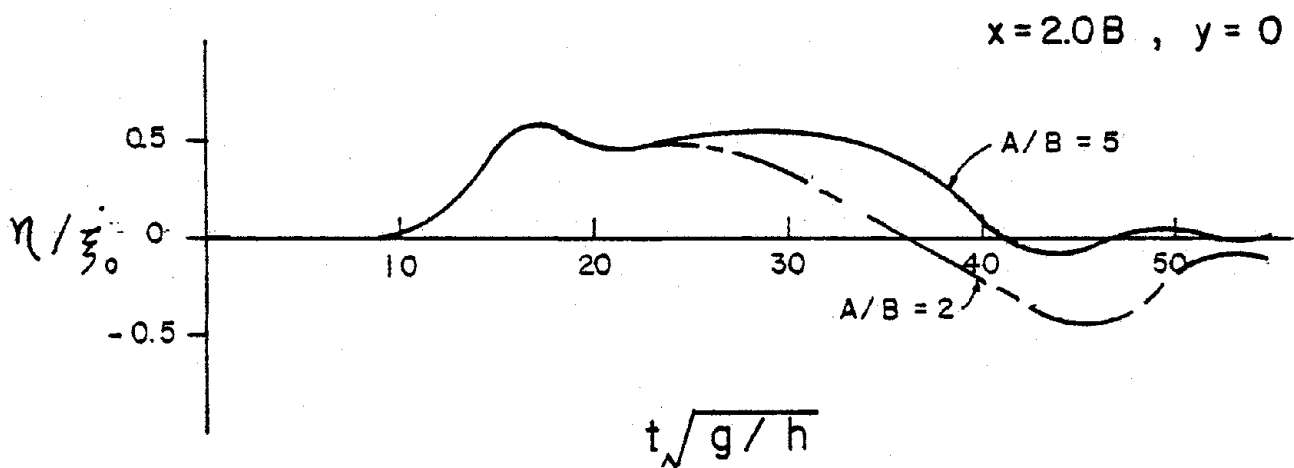
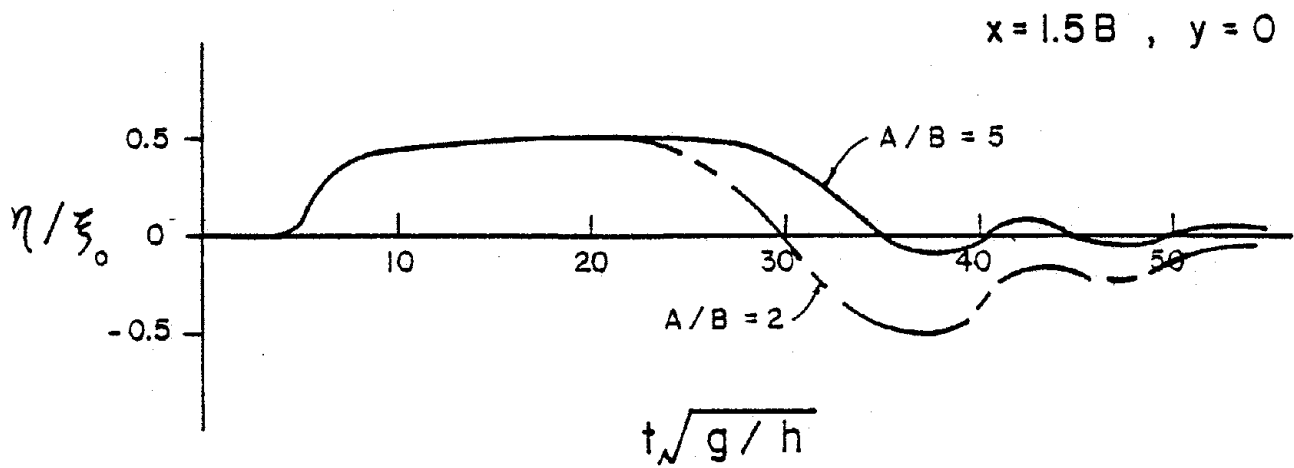
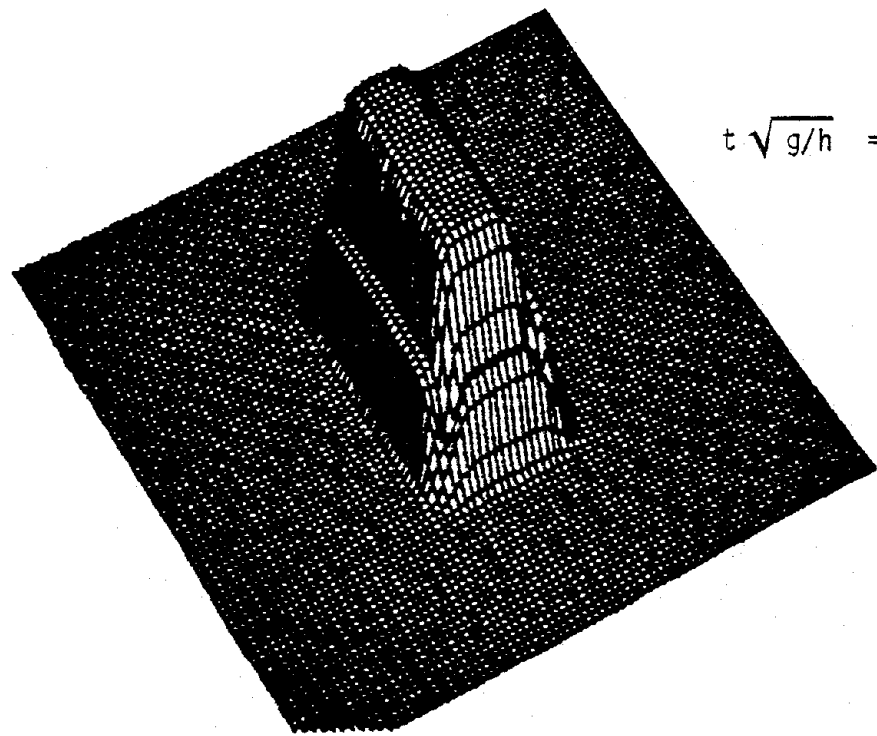
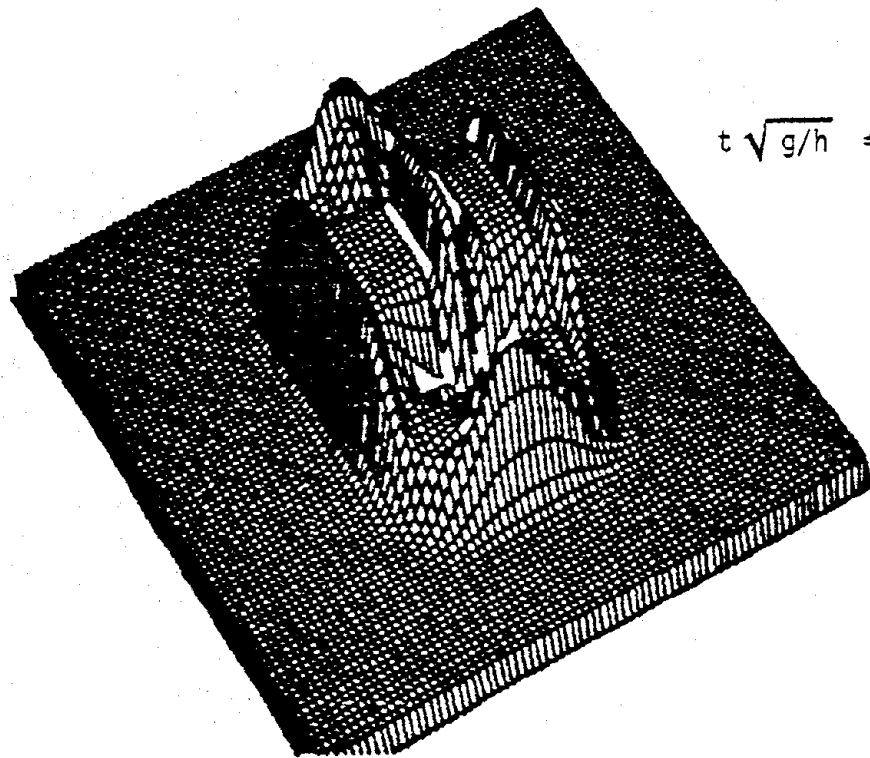


FIG. 3 WATER SURFACE PROFILES FOR  $A/B = 5$  AND  $A/B = 2$  AT  $x = 1.5B, 2.0B$  AND  $2.5B; y = 0$

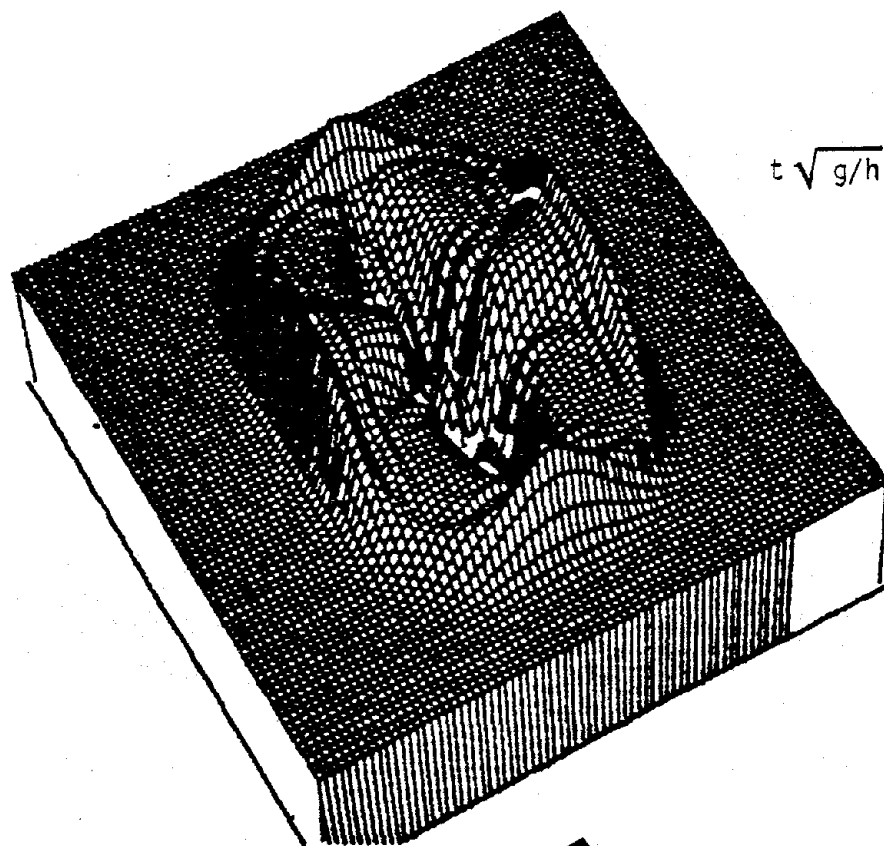


$$t \sqrt{g/h} = 4.20$$

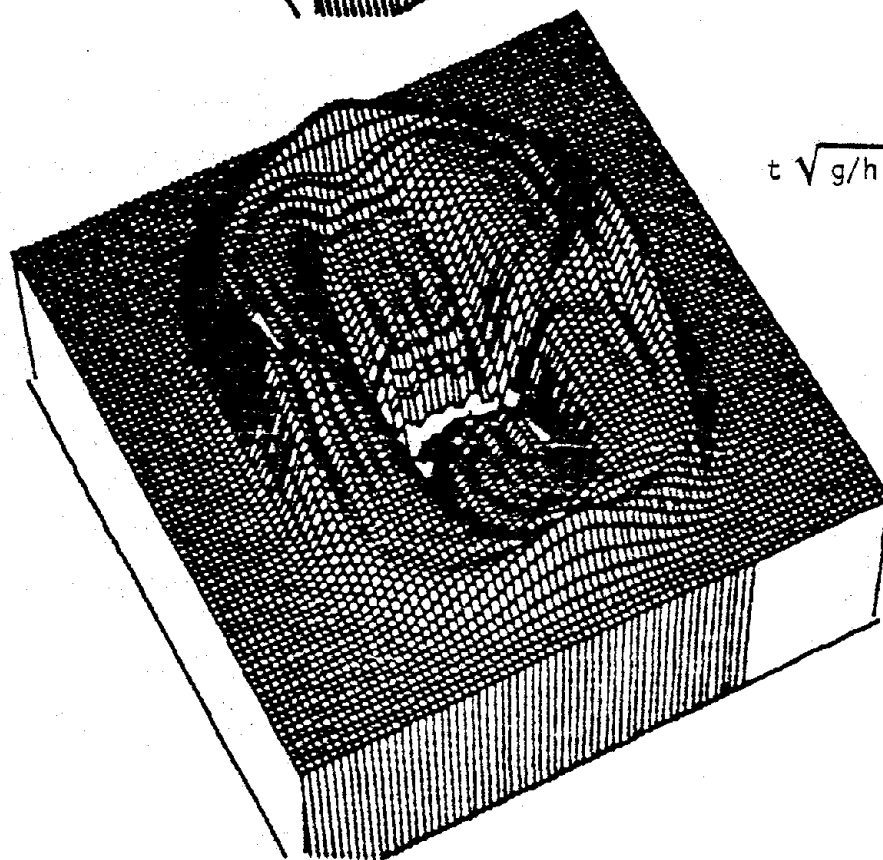


$$t \sqrt{g/h} = 12.61$$

FIG. 4 THREE DIMENSIONAL PICTURES SHOWING THE WAVE AMPLITUDE  $\eta/\xi_0$  NEAR THE GENERATION REGION FOR SPECIFIED TIME PARAMETER (VIEWING ANGLE  $\theta = 60^\circ$ ,  $\delta = 60^\circ$ ) ASPECT RATIO A/B = 2



$t \sqrt{g/h} = 21.02$



$t \sqrt{g/h} = 29.43$

FIG. 5 THREE DIMENSIONAL PICTURES SHOWING THE WAVE AMPLITUDE  $\eta/\xi_0$  NEAR THE GENERATION REGION FOR SPECIFIED TIME PARAMETER (VIEWING ANGLE  $\theta = 60^\circ$ ,  $\delta = 60^\circ$ ) ASPECT RATIO  $A/B = 2$

They represent an overall pictorial view of the wave profile at  $t \cdot \sqrt{g/h} = 4.20, 12.61, 21.02, \text{ and } 29.43$ . The vertical viewing angle for these pictures is  $60^\circ$  and the horizontal angle is  $60^\circ$ . These pictures allow us to visualize the manner by which the waves are transformed from the original form of a parallelepiped into the complicated wave form at some later time.

In order to demonstrate further the transformation of wave profile as a function of time, the water surface profile along a certain axis is also obtained. Figure 6 shows the water surface profile along x axis ( $y = 0, \text{ for } x > 0$ ) for two length/width ratio:  $A/B = 5, 2$ . They are obtained by cutting the three-dimensional pictures such as that shown in Figures 4 and 5. This series of water surface profiles shows how waves are propagated from the origin of disturbance toward the surrounding region. Using these wave profiles, we can compute the propagation speed as 2.2 ft/sec. This propagation speed is very close to the long wave celerity  $C = \sqrt{gh} = 2.3 \text{ fps}$ . From

Figure 6 we can see that the water surface profile is the same for  $A/B = 5$  and 2 for  $t\sqrt{g/h} < 16.81$ . At a later time, the water surface profile differs significantly, especially at the tail region. However, the leading wave portion is quite similar in both cases for the time variables presented.

Water surface profiles along the y axis are presented in Figure 7 for two different values of  $A/B$  for various dimensionless time parameters,  $t\sqrt{g/h}$ . The region where  $y = A$  is marked for reference. By examining this series of wave profiles, a number of observations can be made:



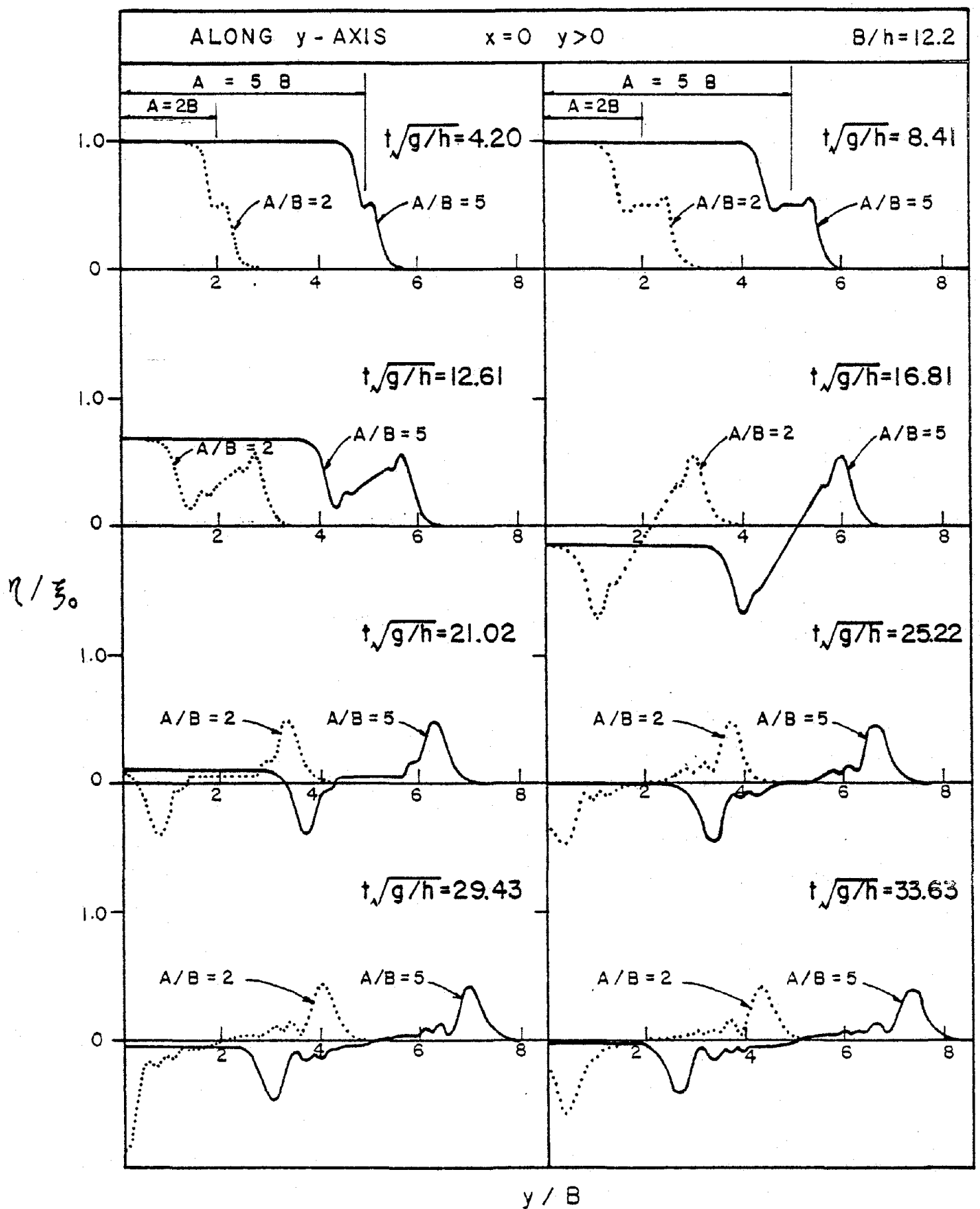


FIG. 7 WATER SURFACE PROFILES FOR TWO LENGTH / WIDTH RATIO ( $A/B = 5$  &  $A/B = 2$ ) AT  $x=0$ ,  $y > 0$

- a. The leading wave is similar for the case of  $A/B = 5$  and  $2$  at almost all the time parameters presented.
- b. A reverse symmetric wave profile with respect to  $y = A$  is found at almost all the time parameters shown. ( $y = A$  corresponds to the edge of the rectangular block).
- c. As waves propagate away from the generation region, interesting wave profile histories in the region  $y < A$  can be found. The leading negative wave which exists within the region  $y < A$  appears to be converging toward the center first and then propagating outward (this can be clearly seen from the curves  $A/B = 2$ ). This further demonstrates that the waves are indeed propagating in every direction resulting in complicated wave profiles, especially when  $A/B$  is small.
- d. The wave profile along the major axis (Figure 7) and that along the minor axis differs considerably for  $t\sqrt{g/h}$  greater than a certain value. (In the example of Figure 6 and 7,  $t\sqrt{g/h} > 12.61$ ).
- e. Due to radiation of waves in every direction, significant modulation of wave profile has already taken place (as evidenced from the curves presented) even though the time parameter  $t\sqrt{g/h}$  is still small. This is one of the aspects that represents a significant departure from the two-dimensional results.

The numerical method used for computing the waves generated through the impulsive bed upthrust of a rectangular block is much more efficient than the direct integration method. For a particular time parameter, to obtain the wave profiles for an array of  $256 \times 256$  data points (in the  $x$ - $y$  plane) would require only 37 seconds of CPU time on a DEC-10 computer. Using this data, one can then construct the three-dimensional picture of the water surface elevation such as those presented in Figures 4 or 5.

## 5. Concluding Remarks

An effective numerical method has been presented in this paper. The method is used to compute the water waves generated through the impulsive bed upthrust of a rectangular block of varying ratio of major axis/minor axis (A/B). Three-dimensional pictures showing water surface elevation in the x-y plane for a certain specified time parameter have been shown. For the cases computed, along with the time parameter presented, the leading wave shape was similar for the different ratios of A/B. However, the water surface profile of the tail region differs considerably as A/B is reduced. The wave profile along the major axis and that along the minor axis differs considerably for  $t\sqrt{g/h}$  greater than a certain value in all cases.

As can be inferred from the results presented in this paper, the three-dimensional effect is quite significant, even with the assumed simple bed deformation. Therefore, in order to more fully understand the nature of tsunamis due to a submarine earthquake, one must take into account the three-dimensional effect.

## References

1. H.C. Andrews, Computer Techniques in Image Processing, Academic Press, New York, 1970.
2. E.O. Brigham, The Fast Fourier Transform, Prentice-Hall Inc., Englewood Cliffs, New Jersey, 1974.
3. P.V.D. Driessche and R.D. Braddock, "On the Elliptic Generating Region of a Tsunami," Journal of Marine Research, Australia, 1972, pp. 217-226.
4. J.L. Hammack, "A Note on Tsunamis: Their Generation and Propagation in an Ocean of Uniform Depth," Journal of Fluid Mechanics, Vol. 60, Part IV, 1973, pp. 769-799. (For more detail, see Report No. KH-R-28, W. M. Keck Laboratory of Hydraulics and Water Resources, California Institute of Technology, Pasadena, California, 1972).
5. K. Horikawa, Coastal Engineering - An Introduction to Ocean Engineering, John Wiley & Sons, New York, 1978, Chapter 3.
6. K. Kajiura, "The Leading Wave of a Tsunami," Bulletin of the Earthquake Research Institute, Tokyo University, Vol. 41, 1963, pp.535-571.
7. K. Kajiura, "Tsunami Source, Energy and the Directivity of Wave Radiation," Bulletin of the Earthquake Research Institute, Tokyo University, Vol. 48, 1970, pp. 835-869.
8. A.V. Oppenheim and R.W. Schafer, Digital Signal Processing, Prentice-Hall Inc., Englewood Cliffs, New Jersey, 1975.
9. I.S. Reed, T.K. Truong, Y.S. Kwoh and E.L. Hall, "Image Processing by Transforms over a Finited Field," IEEE Transaction on Computers, Vol. C-20, No. 9, 1977.
10. W.G. Van Dorn, "Tsunamis," Advances in Hydroscience, Vol. 2, 1965, pp. 1-48.

### 3. 1. INTRODUCTION

In recent years finite-amplitude, shallow-water waves have been under intensive investigation. Korteweg - de Vries equation (1895) have long been found to describe the propagation of moderate amplitude waves in relatively shallow water of uniform depth. Exact solution, asymptotic solution, as well as numerical solution of the KdV equation can be found in various publications e.g. Gardner et al (1967), Segur (1973), Johnson (1972, 1973), Vliegenthart (1971) and Whitham (1974). Experiments have also been conducted to test the validity of the KdV equation as a propagation model in shallow water such as reported by Zabusky & Galvin (1971), Hammack (1973), Hammack & Segur (1974).

In these theoretical and numerical studies the fluid is considered inviscid, thus the effects of non-linearity and dispersiveness are included while the dissipation effect is neglected. The present study attempts to find an approximate governing equation if the viscosity of the fluid is included in the analysis. This is motivated by the apparent deviation of the results from the laboratory experiments compared with the inviscid theories as illustrated by Hammack (1973).

Most recently two separate studies on the modified KdV equation, independent of the present work, have just appeared in the literatures: these are the work of Shuto (1976) and Miles (1976). Shuto included a turbulent boundary stress based on experimentally determined friction coefficient. Miles considered the laminar boundary layer and derived a modified KdV equation that involves an integral operator. The results of Miles show that the damping

coefficient is inversely proportional to the square root of an appropriate Reynold's number which is also demonstrated in the present work.

The viscous dissipation effect on the wave system can be found in three areas: internal viscous dissipation, viscous boundary layer at the free surface and viscous boundary layer at the bottom. In the present study, the viscous boundary layer at the free surface is neglected. The internal viscous dissipation is shown to be small compared with the bottom friction. Numerical solutions of the derived viscous KdV equation for various initial conditions have been obtained and compared with the experimental results of Hammack (1973) and Hammack & Segur (1974).

3.2. THEORETICAL ANALYSIS

For the theoretical analysis, the flow is considered two-dimensional and the fluid incompressible.

The governing equations are the Navier-Stokes equations and the continuity equation:

$$\frac{\partial u^*}{\partial t^*} + u^* \frac{\partial u^*}{\partial x^*} + v^* \frac{\partial u^*}{\partial y^*} = -\frac{1}{\rho} \frac{\partial p^*}{\partial x^*} + \nu \left( \frac{\partial^2 u^*}{\partial x^{*2}} + \frac{\partial^2 u^*}{\partial y^{*2}} \right) \quad \dots (1-a)$$

$$\frac{\partial v^*}{\partial t^*} + u^* \frac{\partial v^*}{\partial x^*} + v^* \frac{\partial v^*}{\partial y^*} = -\frac{1}{\rho} \frac{\partial p^*}{\partial y^*} - g + \nu \left( \frac{\partial^2 v^*}{\partial x^{*2}} + \frac{\partial^2 v^*}{\partial y^{*2}} \right) \quad \dots (1-b)$$

$$\frac{\partial u^*}{\partial x^*} + \frac{\partial v^*}{\partial y^*} = 0 \quad \dots (1-c)$$

where  $u^*$  and  $v^*$  are the horizontal ( $x^*$ ) and vertical ( $y^*$ ) components of fluid velocity respectively,  $p^*$  the pressure,  $\rho$  the fluid density,  $\nu$  the kinematic viscosity,  $g$  the gravitational acceleration,  $d$  the water depth,  $t^*$  the time and  $L$  the characteristic horizontal length.

If the physical parameters in the Navier-Stokes equations are non-dimensionalized as:

$$x = \frac{x^*}{L}, \quad y = \frac{y^*}{d}, \quad \delta = \frac{d}{L}, \quad u = \frac{1}{\epsilon} \frac{u^*}{\sqrt{gd}}, \quad v = \frac{1}{\epsilon} \frac{Lv^*}{d\sqrt{gd}}, \quad t = \frac{\sqrt{gd}}{L} t^*,$$

$$p = \frac{1}{\epsilon} \left[ y - 1 + \frac{p^* - p_0^*}{\rho gd} \right], \quad \beta = \frac{L\nu}{d^2\sqrt{gd}}, \quad \epsilon = \frac{\eta_0^*}{d}, \quad (1-d)$$

where  $p_0^*$  is the atmospheric pressure, and  $\epsilon$  is the amplitude parameter defined as the maximum wave amplitude  $\eta_0^*$  divided by the water depth  $d$ .

Then the governing equations can be reduced to the following dimensionless form:

$$u_t + \epsilon u u_x + \epsilon v u_y + p_x = \beta u_{yy} + \beta \kappa \epsilon u_{xx} \quad (2a)$$

$$\kappa \epsilon (v_t + \epsilon u v_x + \epsilon v v_y) + p_y = \beta \kappa \epsilon v_{yy} + \beta \kappa^2 \epsilon^2 v_{xx} \quad (2b)$$

$$u_x + v_y = 0 \quad (2c)$$

In which the parameter  $\delta^2 = \kappa \epsilon$  with  $\kappa = O(1)$  is introduced; this implies that the effect of dispersion and non-linearity is equally important.

The boundary conditions are as follows:

(i) at the sea bottom there must be no slip,

$$\text{i.e. } u = v = 0 \quad \text{at } y = 0$$

(ii) at the free surface  $y = 1 + \epsilon \eta$ , the free surface condition must be satisfied.

$$\begin{cases} v = \eta_t + \epsilon u \eta_x \\ 1 - y + \epsilon \eta = 0 \end{cases}$$

In order to facilitate further development and the eventual numerical calculation, the following characteristic coordinates are used:

$$\xi = x - t; \quad \tau = \epsilon x$$

The dependent variables  $u$ ,  $v$ ,  $p$  are expanded in a power series of  $\epsilon$  such as:

$$u = u^0 + \epsilon u^1 + \epsilon^2 u^2 + \dots$$

Substitute these power series into Eq. 2, we can collect the following equations with different order of approximation.

Zeroth order ( $\epsilon^0$ ) approximation:

$$\begin{aligned}
 u_{\xi}^0 &= p_{\xi}^0 + \beta u_{yy}^0 \\
 p_y^0 &= 0
 \end{aligned}
 \tag{3}$$

$$u_{\xi}^0 + v_y^0 = 0$$

with the boundary condition

$$\left. \begin{aligned}
 p^0 &= \eta^0 \\
 v^0 &= -\eta \frac{\partial}{\partial \xi} \\
 u_y^0 &= 0
 \end{aligned} \right\} \text{ at } y = 1$$

$$v^0 = 0, \text{ at } y = 0$$
(4)

The solution of these  $\epsilon^0$  order equations is that of the linear shallow water wave theory; thus, the horizontal velocity  $u^0$  will be uniform in  $y$  which will violate the non-slip condition at the sea bottom. This must be corrected at the next order's approximation in order to satisfy the non-slip condition in  $u$  at the bottom.

First order ( $\epsilon^1$ ) approximation:

$$\begin{aligned}
 -u \frac{1}{\xi} + u^0 u_{\xi}^0 + v^0 u_y^0 + p_{\tau}^0 + p_{\xi}^1 &= \beta u_{yy}^0 + \kappa \beta u_{\xi\xi}^0 \\
 -\kappa v_{\xi}^0 + p_y^1 &= \kappa \beta v_{yy}^0 \\
 u_{\tau}^0 + u_{\xi}^1 + v_y^1 &= 0
 \end{aligned}
 \tag{5}$$

with the boundary condition

$$\left. \begin{aligned}
 p^1 &= \eta^1 \\
 \eta^0 \frac{\partial v^0}{\partial y} + v^1 &= -\eta_\xi^1 + u^0 \eta_\xi^0 \\
 u_y^1 &= 0
 \end{aligned} \right\} \text{at } y = 1 \quad (6)$$

$$\left. \begin{aligned}
 v^1 &= 0 \\
 u^1 &= -\frac{u^0}{\varepsilon}
 \end{aligned} \right\} \text{at } y = 0$$

Solving these equations, with integration performed from the bottom to the free surface with respect to  $y$  and assuming  $\partial u / \partial y$  at the free surface as zero (this assumption implies that the dissipation due to boundary layer at the free surface is neglected) we obtain the following equation for  $\eta_0$ :

$$\eta_\tau^0 + \frac{3}{2} \eta^0 \eta_\xi^0 + \frac{\kappa}{6} \eta^0_{\xi\xi\xi} = \frac{\kappa}{2} \beta \eta^0_{\xi\xi} - \frac{\beta}{2} u_y^1 \Big|_{y=0} \quad (7)$$

with  $\beta = 0$ , Eq. (7) is the well known KdV equation. The term  $u_y^1$  in Eq. 7 represents the velocity gradient at the bottom and it must be evaluated. It should be noted here that the first term in the right hand side of Eq. 7 represents the internal viscous dissipation while the second term represents the dissipation at the bottom. As we recall for approximation to the  $\varepsilon^1$  order

$$u = u^0 + \varepsilon u^1, \quad u^1 = \frac{1}{\varepsilon} (u - u^0)$$

Thus  $\left. \frac{u^1}{y} \right|_{y=0} = \frac{1}{\varepsilon} \left. \frac{u}{y} \right|_{y=0}$  because we allow  $u^0$  to

be independent of  $y$  in the zeroth order approximation.

Rearranging the first equation of Eq. (5) and noting that  $u^0$  and  $\eta^0$  are interchangeable, we have

$$\frac{1}{\varepsilon} (u - u^0)_{\xi} = (n^0 \eta_{\xi}^0 + \eta_{\tau}^0 + p_{\xi}^1 - \kappa \beta n_{\xi\xi}^0) - \frac{\beta}{\varepsilon} (u - u^0)_{yy} \quad (8)$$

By retaining only the most important terms (which are the terms on the left hand side and the last term on the right hand side) we obtain a linear equation for the boundary layer region close to the bed:

$$(u - u^0)_{\xi} = -\beta (u - u^0)_{yy} \quad (9)$$

with the boundary condition:

$$\begin{aligned} u - u^0 &= -u^0 & \text{at } y = 0 \\ u - u^0 &= 0 & \text{at } y \rightarrow \infty \text{ (beyond the edge of the} \\ & & \text{boundary layer)} \end{aligned} \quad (10)$$

Eq. (9) is a heat equation, the solution of such an equation is quite well known and can be expressed in a Fourier integral or most conveniently in the Duhamel's form (e.g. see Webster (1955) p. 173):

$$u - u^0 = -\frac{2}{\sqrt{\pi}} \int_0^{\infty} F\left(\xi + \frac{y^2}{4\beta\gamma^2}\right) e^{-\gamma^2} d\gamma \quad (11)$$

in which the boundary value  $u^0$  at  $y = 0$  is assigned to be  $u^0 = F(\xi)$ .

In order to further carry out the integration of Eq. 11 we have to assume a functional form for  $F$ . We choose

$u^0 = F(\xi) = A \operatorname{sech}^2 \xi$  as a representative form.

$$\text{Then } u - u^0 = - \frac{2A}{\sqrt{\pi}} \int_0^{\infty} \operatorname{sech}^2 \left( \xi + \frac{y^2}{4B\gamma^2} \right) e^{-\gamma^2} d\gamma \quad (12)$$

differentiation with respect to  $y$  and evaluate this value at  $y = 0$

we obtain:

$$\begin{aligned} \left. \frac{\partial u}{\partial y} \right|_{y=0} &= \frac{4A \operatorname{sech}^2 \xi}{\sqrt{\pi B}} \int_0^{\infty} \frac{\tanh(\xi + \bar{\alpha}^2) d\bar{\alpha}}{(\cosh \bar{\alpha}^2 + \tanh \xi \sinh \bar{\alpha}^2)^2} \\ &= \frac{4u^0}{\sqrt{\pi B}} C(\xi) = \frac{4\eta^0}{\sqrt{\pi B}} C(\xi) \end{aligned} \quad (13)$$

The function  $C(\xi)$ , which represents the integral in the above equation, can be evaluated numerically for different value of  $\xi$  and is presented in Fig. 1. As can be seen from Fig. 1, the function  $C(\xi)$  approaches an asymptotic value of 0.62 very quickly. Herein we will use 0.62 for  $C(\xi)$ , therefore, Eq. (13) and the last term of Eq. 7 can be further simplified:

$$\begin{aligned} \left. \frac{\partial}{\partial y} \left( \frac{\beta}{2} \frac{\partial u^1}{\partial y} \right) \right|_{y=0} &= \left. \frac{\beta}{2\varepsilon} \frac{\partial u}{\partial y} \right|_{y=0} \\ &= \frac{0.7 \sqrt{\beta}}{\varepsilon} \eta^0 = \alpha \eta^0 \end{aligned} \quad (14)$$

For an experimental wave tank of width  $W$  in water depth  $d$ , the value of  $\alpha$  should be multiplied by  $1 + 2d/W$  to account for the additional frictional effect at the side walls.

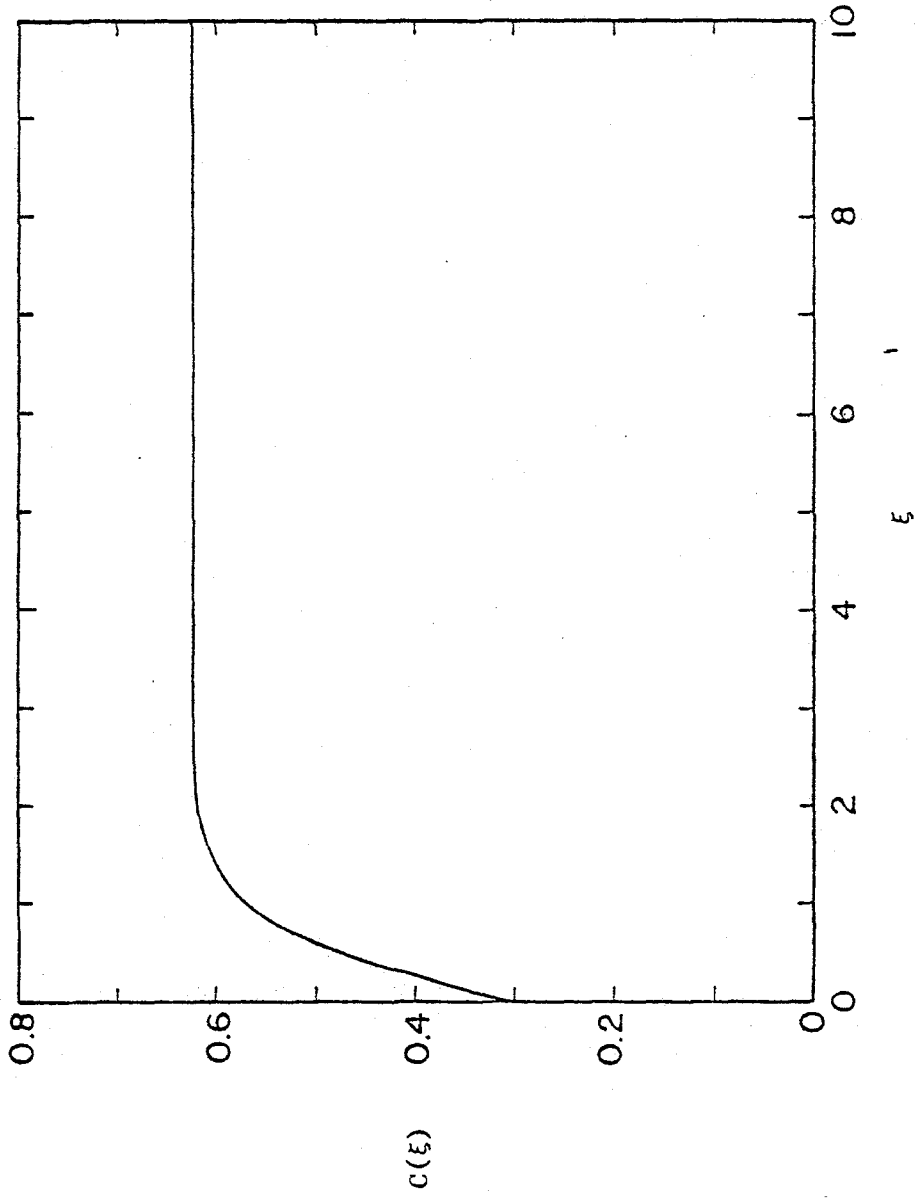


Fig. 1. Numerically integrated function  $C(\xi)$  as defined in Eq. 13.

Therefore, Eq. (7) can be rewritten as:

$$\eta_{\tau}^{\circ} + \frac{3}{2}\eta^{\circ}\eta_{\xi}^{\circ} + \frac{\kappa}{6}\eta_{\xi\xi\xi}^{\circ} = a\eta_{\xi\xi}^{\circ} - \alpha\eta^{\circ} \quad (15)$$

where  $a = \frac{\kappa\beta}{2}$ . For most cases,  $a \ll \alpha$  and "a" can be neglected, it is kept to this point to demonstrate the mechanism of internal viscous dissipation.

It is interesting to discuss Eq. 15 further by neglecting the term  $a\eta_{\xi\xi}^{\circ}$  and make the transformation  $\tilde{\eta} = \eta e^{\alpha\tau}$ . Then we can get a KdV equation with modified coefficients:

$$\tilde{\eta}_{\tau} + \frac{3}{2}(e^{-\alpha\tau})\tilde{\eta}\tilde{\eta}_{\xi} + \frac{\kappa}{6}\tilde{\eta}_{\xi\xi\xi} = 0 \quad (16)$$

Eq. (16) demonstrates that the net effect of the boundary dissipation is to gradually decrease the influence of the non-linear term. Because a solitary wave is a solution of the KdV equation, we can now expect for a very small value of  $\alpha\tau$ , the amplitude of a solitary wave will decay as  $e^{-\alpha\tau}$ . As  $\alpha\tau$  increases,  $\eta$  should decay faster. In fact, it can be shown, e.g. Ott and Sudan (1970), Ostrovskiy and Pelinovskiy (1974), that the amplitude decay of a solitary wave follows the form:

$$\frac{\eta(\tau)}{\eta(0)} = e^{-\frac{4}{3}\alpha\tau} \quad (17)$$

Thus, for the present case, if  $\alpha$  is evaluated from Eq. 14, then the amplitude decay of a solitary wave can be conveniently estimated from Eq. 17. Results from this simple process agree extremely well with the numerical results and the prior published theories on damping of solitary wave (i.e. Keulegan 1948, Ippen and Kulin 1955). This will be discussed in detail in the results section.

For a more complicated initial wave form, numerical solution of Eq. 15 can be obtained. (For all practical purpose, the coefficient  $a$  in Eq. 15 can be set equal to zero). Examples for this application will be shown in the results section. The finite difference form of Eq. 15 as well as some information concerning the computational aspect is presented in the Appendix.

3. 3. PREVIOUS THEORIES ON DAMPING OF SOLITARY WAVES:

Keulegan (1948) analyzed the rate of loss of energy due to viscous shear within the laminar boundary layer beneath the solitary wave on a smooth surface. For a single solitary wave with an initial maximum amplitude  $(\eta_o)_i$  at  $x = 0$  in water of depth  $d$  and a tank of width  $W$ , he found that the maximum amplitude  $\eta_o$  of the solitary wave at any downstream position  $x$  could be approximated by

$$\frac{\eta_o}{\eta_{oi}} = \left[ 1 + \theta \left( \frac{\eta_{oi}}{d} \right)^{1/4} \right]^{-4} \quad (18)$$

where  $\theta = \frac{1}{12} \left( 1 + \frac{2d}{W} \right) \left( \frac{\nu^2}{gd^3} \right)^{1/4} \left( \frac{x}{d} \right)$  and  $\nu$  is the kinematic viscosity of fluid.

As  $W \rightarrow \infty$ , the above equation can be simplified to become:

$$\eta_o^{-1/4} - (\eta_{oi})^{-1/4} = 0.083 \left( \frac{\nu}{\sqrt{g}} \right)^{1/2} \left( \frac{x}{d^2} \right) \quad (19)$$

It should be noted that  $x$  used here and after represents the horizontal distance from the initial station; therefore, it is equivalent to  $x^*$  used in previous section.

Based on the laboratory data conducted by various investigators, as summarized by French (1969), Eq. 19 seems to overpredict the viscous damping but generally yields reasonably good agreement.

The data of Ippen, Kulin & Raza (1955) also indicate that Keulegan's formula predicts more damping than observed. A separate dissipation study has also been made through direct measurement of bottom shear stress by Ippen and Mitchell (1957). For smooth bed, the mean resistance coefficient  $C'_{fo}$  was found to be related to a wave Reynold number  $R'_{so}$  as follows (see Ippen (1966)):

$$\begin{aligned}
C'_{fo} &= \frac{1.328}{(R'_{so})^{1/2}} = \frac{1.328}{\left(\int_0^\infty \frac{u^2}{\nu} dt\right)^{1/2}} = \frac{1.328}{\left(\frac{1.54\eta_0\sqrt{g\eta_0}}{\nu}\right)^{1/2}} \\
&= \frac{15}{4} \left(\frac{\eta_0}{d}\right)^{-2} \frac{d\eta_0}{dx} \quad (20)
\end{aligned}$$

Integrating the above equation we can obtain the following equation which is very similar to Keulegan's:

$$(\eta_0)^{-1/4} - (\eta_0)_i^{-1/4} = 0.071 \left(\frac{\nu}{g}\right)^{1/2} \frac{x}{d} \quad (21)$$

It is clear that the only difference between Eqs. 19 & 21 is the first coefficient at the right hand side of the equations. Thus, Eq. 21 should therefore predict a smaller amplitude decay.

Comparison of the results from present study with Eq. 19 and 21 will first be made in the next section.

As a first example for the application of the theoretical development presented in previous section, the propagation of a single solitary wave in a laboratory flume is first studied. Fig. 2 presents the gradual damping of a solitary wave with amplitude/depth = 0.12 in two different water depths ( $d = 3$  in. and 6 in.). Numerical solution of Eq. 15 is compared with the theories by Keulegan (Eq. 19) and Ippen and Kulin (Eq. 21). The result obtained by Eqs. 14 and 17 is also included. As expected, at the very early stage of wave propagation, the decay of the maximum amplitude of the solitary wave is quite close to  $e^{-\alpha t}$ . However, as distance from the initial location is increased the numerical result approach the asymptotic result of Eq. 17 very nicely. The decay of amplitude predicted by Keulegan's formula is consistently larger than that of the Ippen's as well as the present result. However, all results are quite close to each other and demonstrate the same trend. For the 6 in. water depth the amplitude decay at the same  $x/d$  is smaller than that for the case of 3 in. depth because the effect of boundary friction is more significant for shallower depth. By looking at the formula for  $\beta$  and  $\alpha$  (Eqs. 1 and 14), it can be seen that as  $d$  increases the values of  $\beta$  and  $\alpha$  are reduced; therefore, the decay of solitary wave amplitude is reduced for the same  $x/d$ .

Fig. 3 presents amplitude decay of a solitary wave with amplitude/depth = 0.08 as a function of  $x/d$  in water depth of 3 in. and 6 in. The general agreement among various curves can also be seen. Again the Keulegan's formula seems to overpredict the amplitude decay but the difference is indeed quite small.

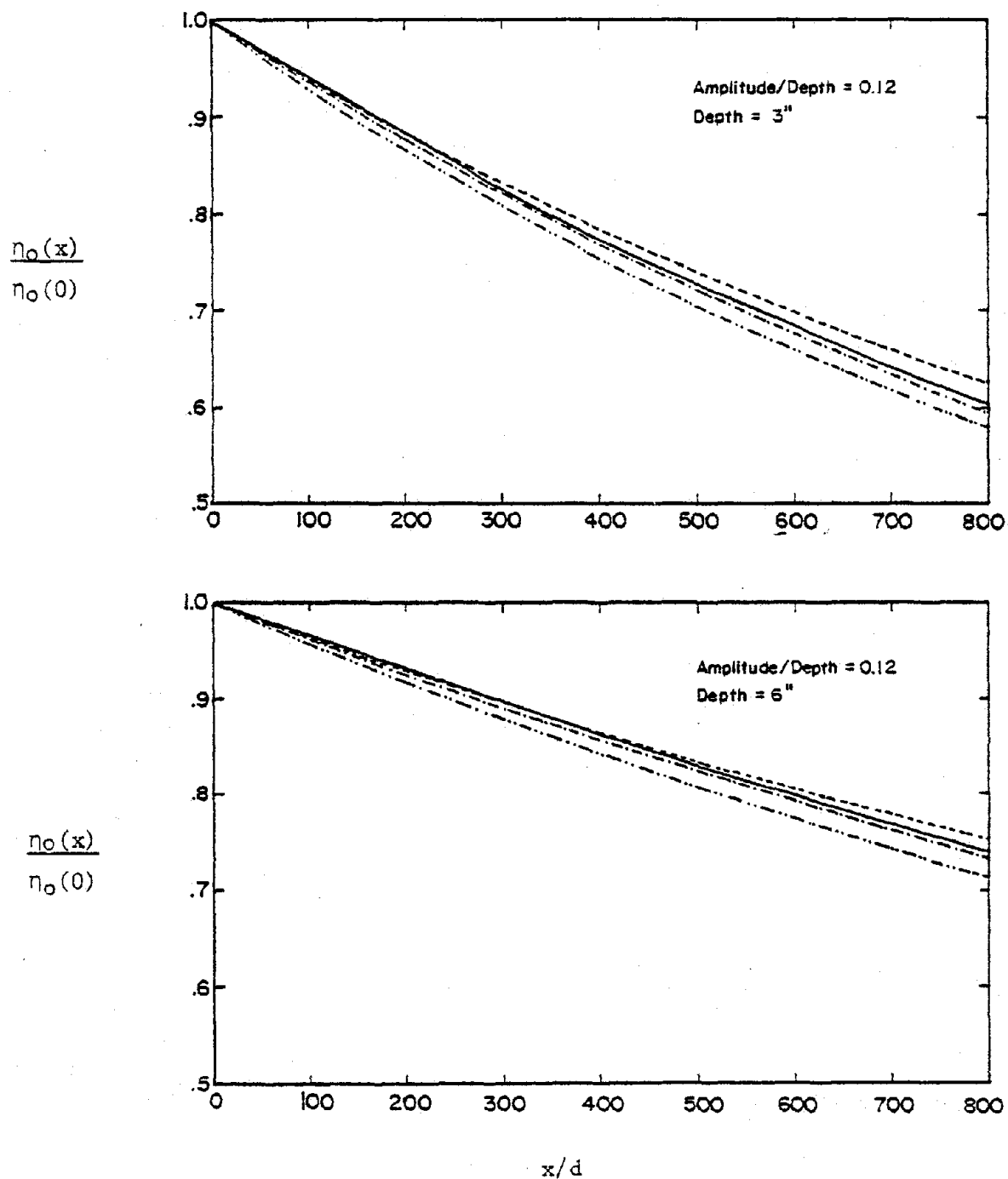


Fig. 2. Amplitude decay,  $\eta_0(x)/\eta_0(0)$ , as a function of horizontal position,  $x/d$ , for a solitary wave with  $\eta_0(0)/d = 0.12$  in two different depths of water.

- present numerical results.
- · - · - · - present results using Eqs. 14 & 17.
- result based on Ippen (1955) (Eq. 21)
- · · - · · - result based on Keulegan (1948) (Eq. 19)

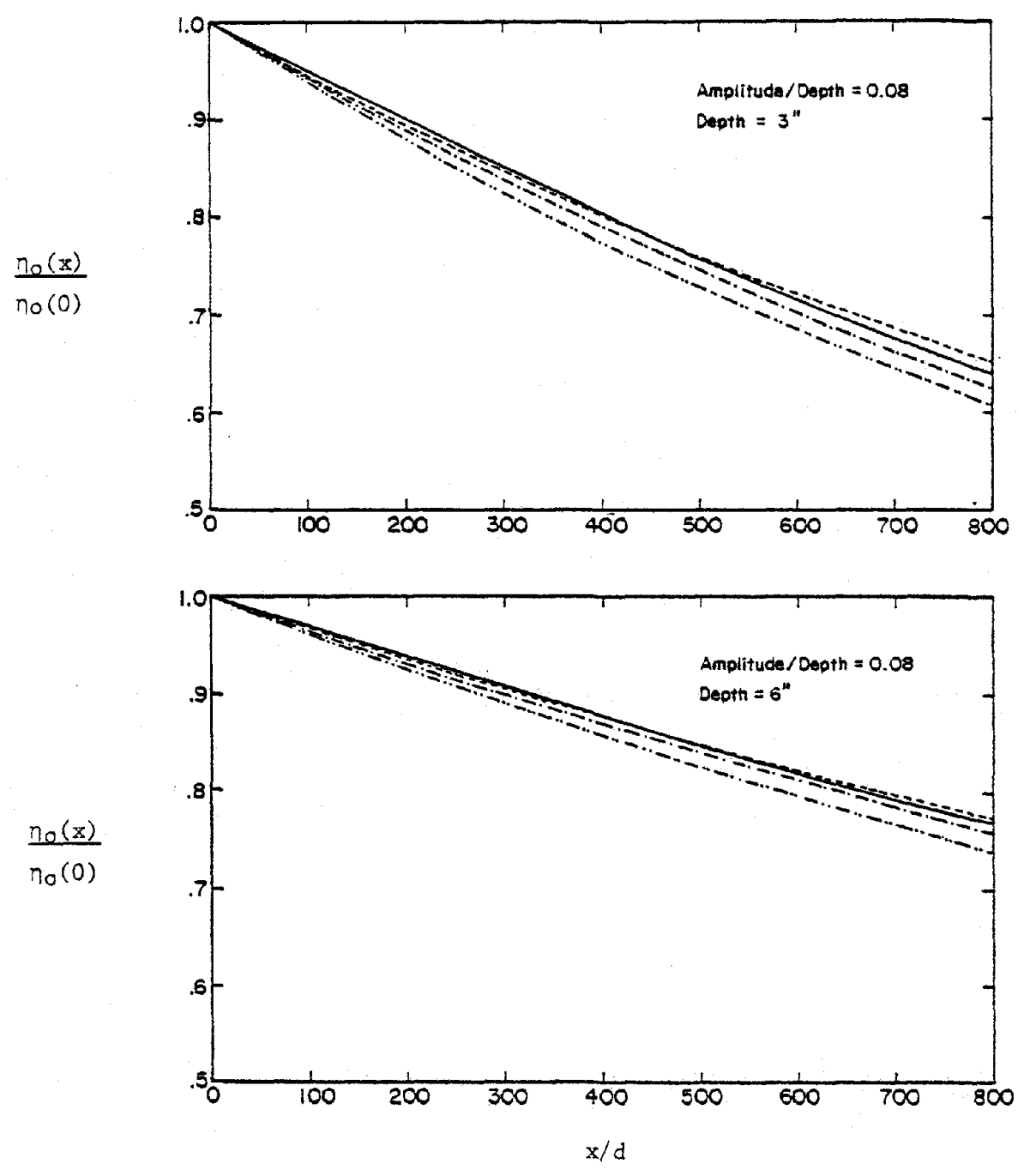


Fig. 3. Amplitude decay,  $\eta_0(x)/\eta_0(0)$ , as a function of horizontal position,  $x/d$ , for a solitary wave with  $\eta_0(0)/d = 0.08$  in two different depths of water.

- present numerical results
- present results using Eqs. 14 & 17
- - - - - result based on Ippen (1955) (Eq. 21)
- · - · - result based on Keulegan (1948) (Eq. 19)

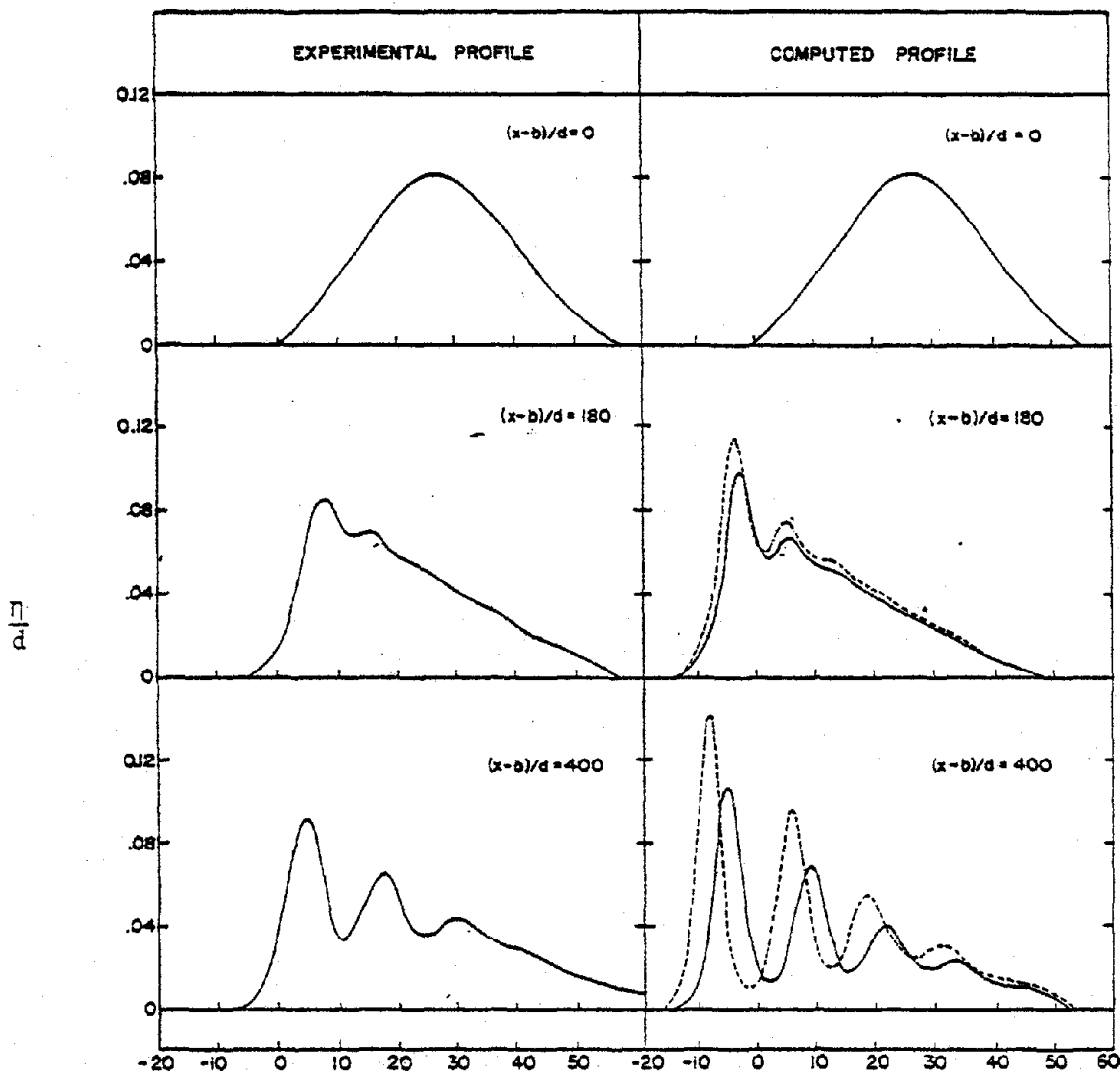
From Figs. 2 and 3, it can be said that the values of  $\beta$  and  $\alpha$  developed in the present study can be used quite conveniently to estimate the amplitude decay of a single solitary wave propagating in shallow water.

Hammack and Segur (1974) conducted very careful and outstanding experiments to test the validity of the KdV equation as a model for moderate amplitude waves propagating in one direction in relatively shallow water of uniform depth. The KdV equation was found to predict accurately the number of evolving solitons and their shapes for initial data whose asymptotic characteristics developed in the test section of the wave tank.

However, the accuracy of the leading-soliton amplitudes computed by the KdV equation could not be conclusively tested owing to the viscous decay of the measured wave amplitude. With the viscous KdV equation developed in the present study, it is interesting to check their experiments with the numerical solution of Eq. 15. This can be considered a more stringent test of the theory as the wave profiles are much more complex than the individual solitary waves considered in Figs. 2 and 3.

The first example of this comparison is shown in Fig. 4. On the left hand side of the figure, the experimental wave profiles from Hammack and Segur (1974) are shown. The initial wave profile is of the type of  $\text{sech}^2$ . As this wave propagates further downstream the initial wave evolves away from the  $\text{sech}^2$  profile. After 180 depths of propagation two local crests can be seen from the experimental data. At 400 depths the observed waves show four local maxima representing 4 solitons although the fourth peak is not as distinguishable as the other three. Their theoretical predictions also show that the number of solitons, that the initial profile eventually evolve into, should be four.

The same initial wave profile is used for the present numerical



$$t \left( \frac{g}{d} \right)^{1/2} - \frac{(x-b)}{d}$$

Fig. 4. Comparison of present numerical wave profiles with the experimental wave profiles of Hammack & Segur (1974) at different stations (water depth  $d = 5$  cm.)

- - - - - inviscid fluid ( $\nu = 0$ )  
 \_\_\_\_\_ water ( $\nu = 1 \times 10^{-5}$  ft<sup>2</sup>/sec.)

solution; these are shown in the right hand side of the figure. The dotted line represents the numerical results of inviscid KdV equation (setting  $a = \alpha = 0$  in Eq. 15) The solid line represents the results from the viscous KdV equation. ( $\alpha = 0.40$  including the side wall correction). As the initial wave propagates to the 180 depths, the deviation of the viscous solution from the inviscid solution is already quite obvious. The effect of the bottom friction is found to reduce the wave amplitude and the propagation speed although the difference in propagation speed is quite small at this point. As wave propagates to 400 depth, the deviation between the inviscid and viscous theory is even more pronounced. Specifically, the inviscid theory predicts the amplitude of the first soliton to be  $0.142d$ , while the viscous theory predicts this amplitude to be  $0.104d$ . The experimental value from Hammack and Segur (1974) showed this amplitude to be  $0.092d$ . It should be noted that from the data of Hammack and Segur the arrival time of the first soliton at 400 depth is 27 sec. The arrival time of the present viscous solution is 26.3 sec which shows a 2.6% difference compared with the experiment. The inviscid theory shows the arrival time of the first crest to be at 26 seconds. The number of soliton is 4 as can be seen from the figure. The time interval between the peaks of soliton agrees very well when comparing the viscous theory and the experiments.

It is interesting to see whether other wave characteristics are modified by the dissipation effect beside the two main features of reducing wave amplitude, slowing propagation speed. To this end, a more detailed plot of the numerical wave profile is shown in Fig. 5 in which fluids with three different viscosities are shown: inviscid fluid ( $\nu = 0$ ), water ( $\nu = 1 \times 10^{-5} \text{ ft}^2/\text{sec}$ ) and crude oil ( $\nu = 6 \times 10^{-5} \text{ ft}^2/\text{sec}$ ). The profiles for the inviscid fluid and water are

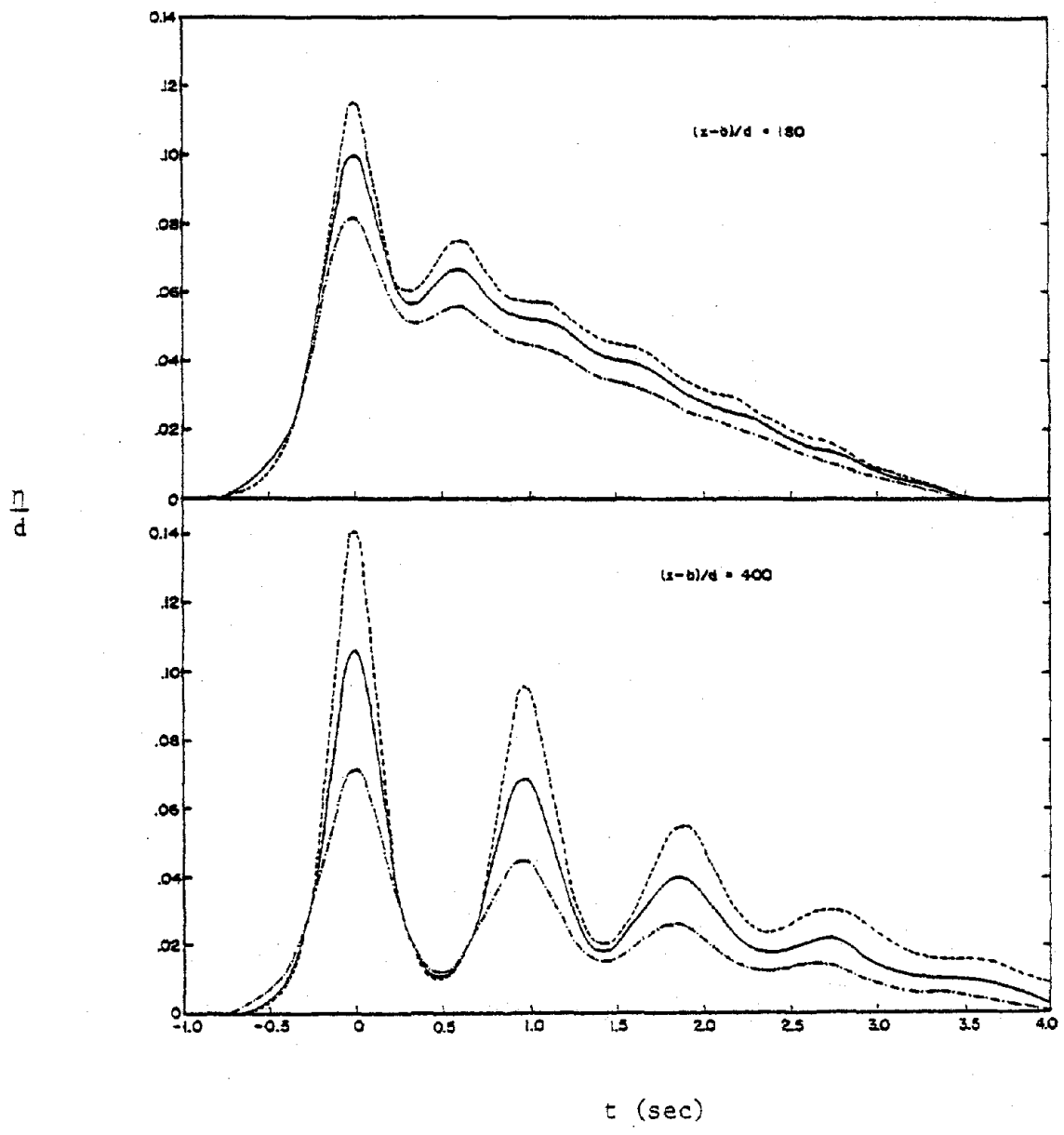


Fig. 5. Comparison of the numerical wave profiles at two stations for these different viscosities:

- inviscid fluid ( $\nu = 0$ )
- water ( $\nu = 1 \times 10^{-5} \text{ ft}^2/\text{sec.}$ )
- . - . - . crude oil ( $\nu = 6 \times 10^{-5} \text{ ft}^2/\text{sec.}$ )

(The initial profile is that shown in Fig. 4).

the same as that shown in Fig. 4 at the corresponding station. The peaks of the first soliton for three different fluids are arranged to be at  $t = 0$ , while the real time scale corresponding to the experiment of Hammack and Segur is used in order to facilitate the comparison. From Fig. 5 it can be seen that the numbers of soliton have not been affected by the viscous effect. The influence on the time interval between soliton peaks is quite small. The amplitude is further reduced as the viscosity of the fluid is increased.

Another example of the wave evolution is shown in Fig. 6. The experimental wave profile is that shown in Hammack and Segur (1974) resulting from a monotonic uplift of the channel bed at  $0 < x < b$  in a water depth of 5 cm. The initial wave profile is approximately a square wave with positive amplitude. As can be seen from the left hand side of Fig. 6, three solitons can be clearly seen from the experimental curve as the wave propagates to 400 depth which is what they have predicted in their theory. The initial experimental wave profile is used as the initial condition for the present analysis except a small portion near the tail end where very small negative oscillations are cut off. As this initial wave propagates to 180 depth, the reduction of wave amplitude due to the dissipation effect is already quite clear although the phase does not change very much. At 400 depth of propagation, the effect of viscosity is quite pronounced. The amplitude of the first soliton is changed from inviscid case of 0.077d to 0.054d for the viscous solution; the arrival time for them differs by about 0.3 second. The amplitude of the second soliton is changed from 0.051d for the inviscid case to 0.037d for viscous case. For the third soliton, the inviscid theory shows an amplitude of 0.021d compared with the viscous theory of 0.014d.

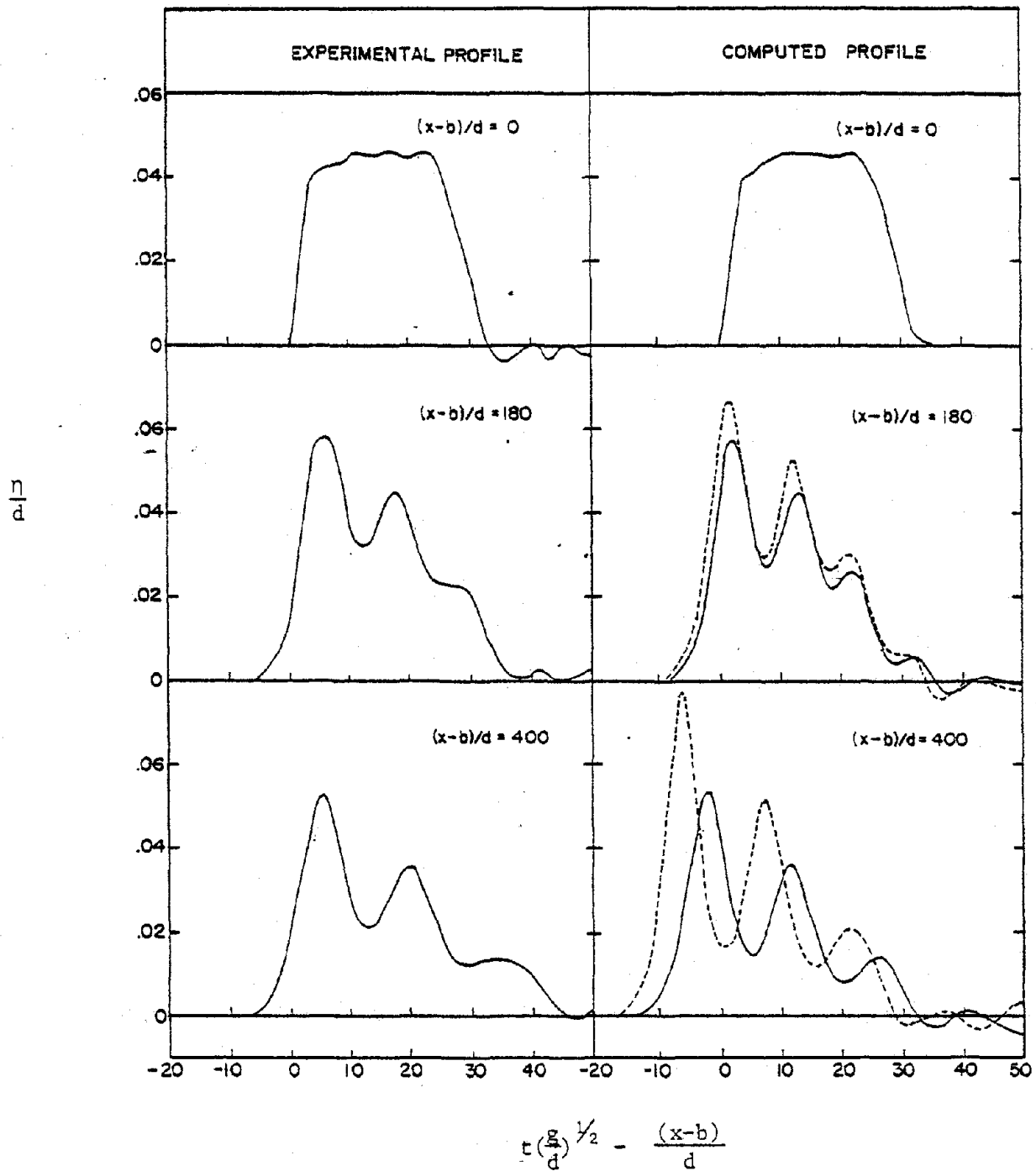


Fig. 6. Comparison of present numerical wave profiles with the experimental wave profiles of Hammack & Segur (1974) at different stations (water depth  $d = 5$  cm.)

- - - - - inviscid fluid ( $\nu = 0$ )  
 \_\_\_\_\_ water ( $\nu = 1 \times 10^{-5}$  ft<sup>2</sup>/sec.)

01

The calculated amplitude for the three solitons agree quite well with the experiments of Hammack and Segur (1974). From their experimental results, the amplitude of the three solitons are: 0.052d, 0.035d, and 0.013d. As in the case of Fig. 4, the arrival time of the viscous soliton is still slightly faster than the experiment. The arrival time of the first peak of the soliton at 400 depth is 27.93 second ( by considering the location of centroid of the wave at 0 depth as the base) compared with 27.46 second for the viscous theory with a difference of 1.7%.

A more detailed wave profile for three different fluids based on the same initial wave profile is shown in Fig. 7. The curves for the inviscid fluid and water ( $\nu = 1 \times 10^{-5} \text{ ft}^2/\text{sec}$ ) are the same as that shown in Fig. 6 at the corresponding location. The first peaks are adjusted to occur at  $t = 0$  for all cases. The curve for crude oil is superimposed to show the effect of viscosity more clearly. As can be seen from the figure the phase has only been changed slightly by different viscosities but the amplitudes of these waves are damped out considerably by viscous dissipation.

Fig. 8 shows the waves resulting from a monotonic downthrow of the channel bed at one end of the wave tank as presented in Hammack and Segur (1974). The initial wave at  $(x - b)/h = 0$  is approximately a negative square wave. As the wave propagates downstream a leading negative wave with decreasing frontal slope followed by an oscillatory wave train can be observed. The computed profiles for both the inviscid and viscous cases based on the initial experimental wave profile are shown on the right hand side of Fig. 8. By comparing the present viscous result with the experimental data surprising good agreement can be seen

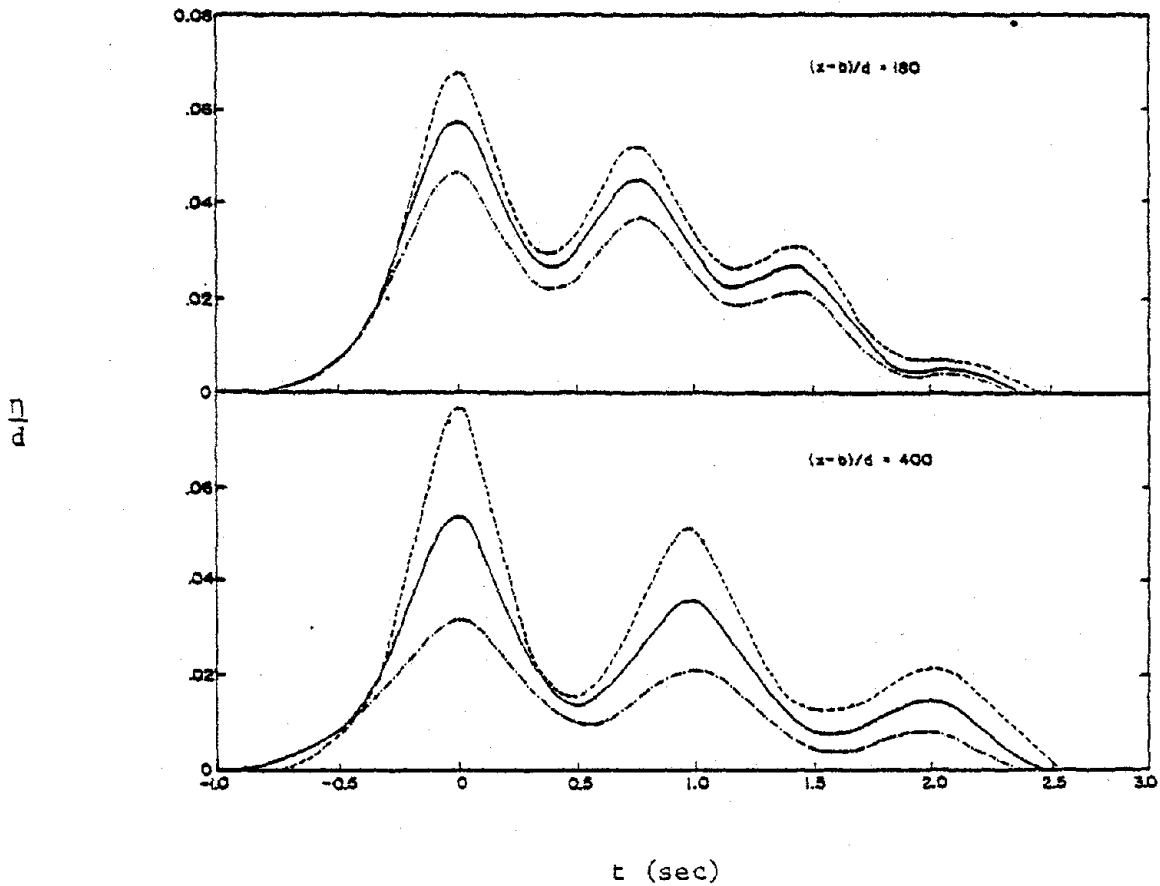


Fig. 7. Comparison of the numerical wave profiles at two stations for three different viscosities:

- - - - - inviscid fluid ( $\nu = 0$ )  
 \_\_\_\_\_ water ( $\nu = 1 \times 10^{-5}$  ft<sup>2</sup>/sec.)  
 - . - . - . crude oil ( $\nu = 6 \times 10^{-5}$  ft<sup>2</sup>/sec.)

(The initial profile is that shown in Fig. 6).

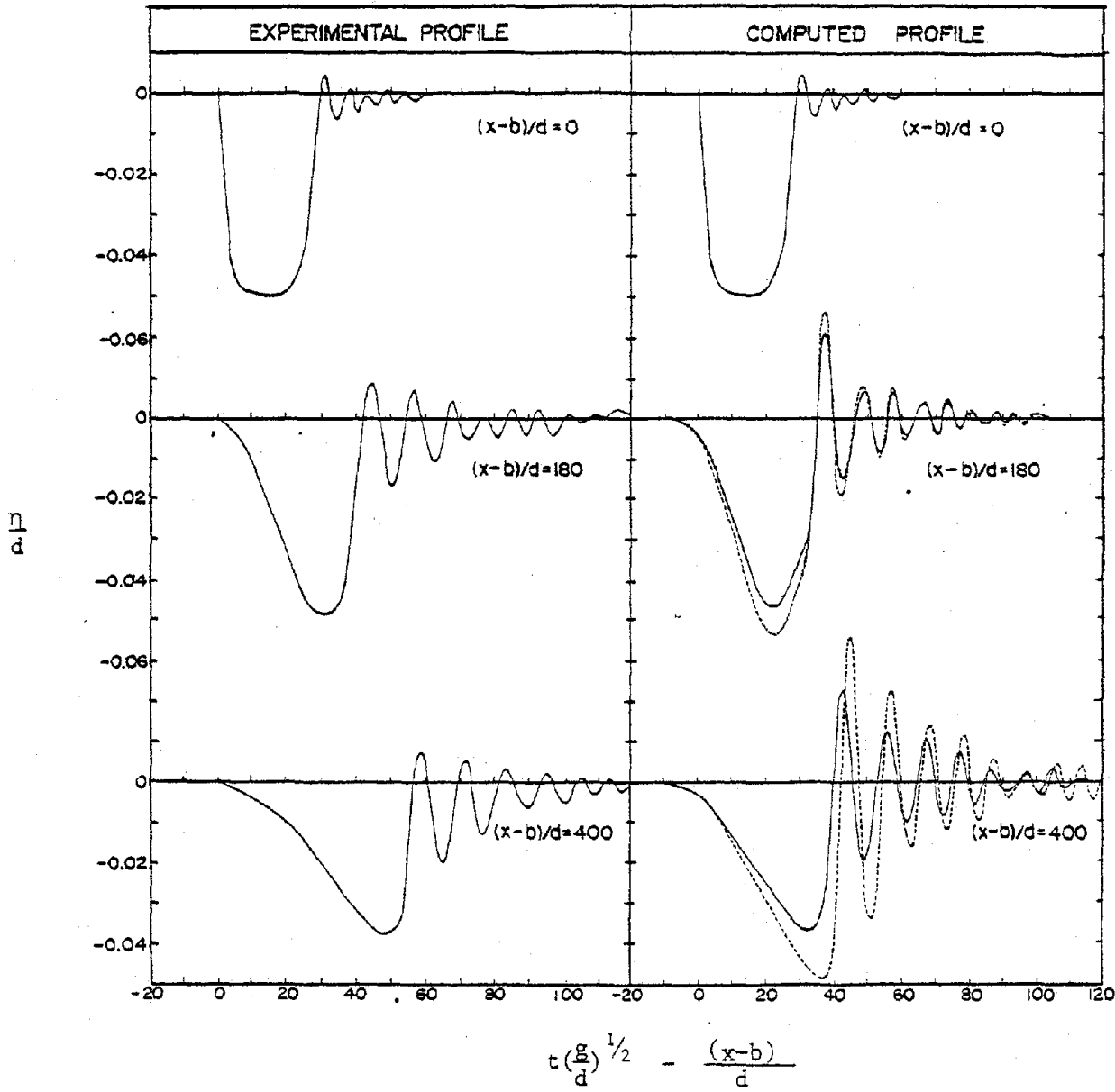


Fig. 8. Comparison of the present numerical wave profiles with the experimental wave profiles of Hammack & Segur (1974) at different stations. (Water depth  $d = 5$  cm.)

- - - - - inviscid fluid ( $\nu = 0$ )  
 \_\_\_\_\_ viscous fluid ( $\nu = 1 \times 10^{-5}$  ft<sup>2</sup>/sec.)

for the leading negative wave amplitude and its length as well as the time interval between the oscillatory waves on the tail end. The dissipation effect for the oscillatory wave tail in the present computation (although significant compared with the inviscid theory) does not adequately account for the total dissipation. In the region consisting oscillatory wave the wave frequency is increased; therefore, mechanism similar to that considered by Van Dorn (1966) should probably be included in order to obtain an even better agreement between the theory and experiments.

A very unusually large, highly nonlinear, negative wave propagating in water depth of 10 cm. is shown in Fig. 9. The experimental wave profiles are taken from Hammack and Segur (1975) and are shown in the left hand side of the figure. The evolution process of this wave is quite complicated and cannot be described by KdV equation alone (see Hammack and Segur (1975)). Therefore, direct comparison of the present computation and the experimental data might be misleading except for the first leading negative wave at which the behavior can probably be modeled by the present viscous KdV equation. Considering these factors, it is somewhat surprising to see that the present numerical result from Eq. 15 actually compared quite well with the experiments except the region where oscillatory waves persist. As mentioned earlier, in future studies additional dissipation mechanism should probably be included for the modulated oscillatory waves behind the leading negative waves.

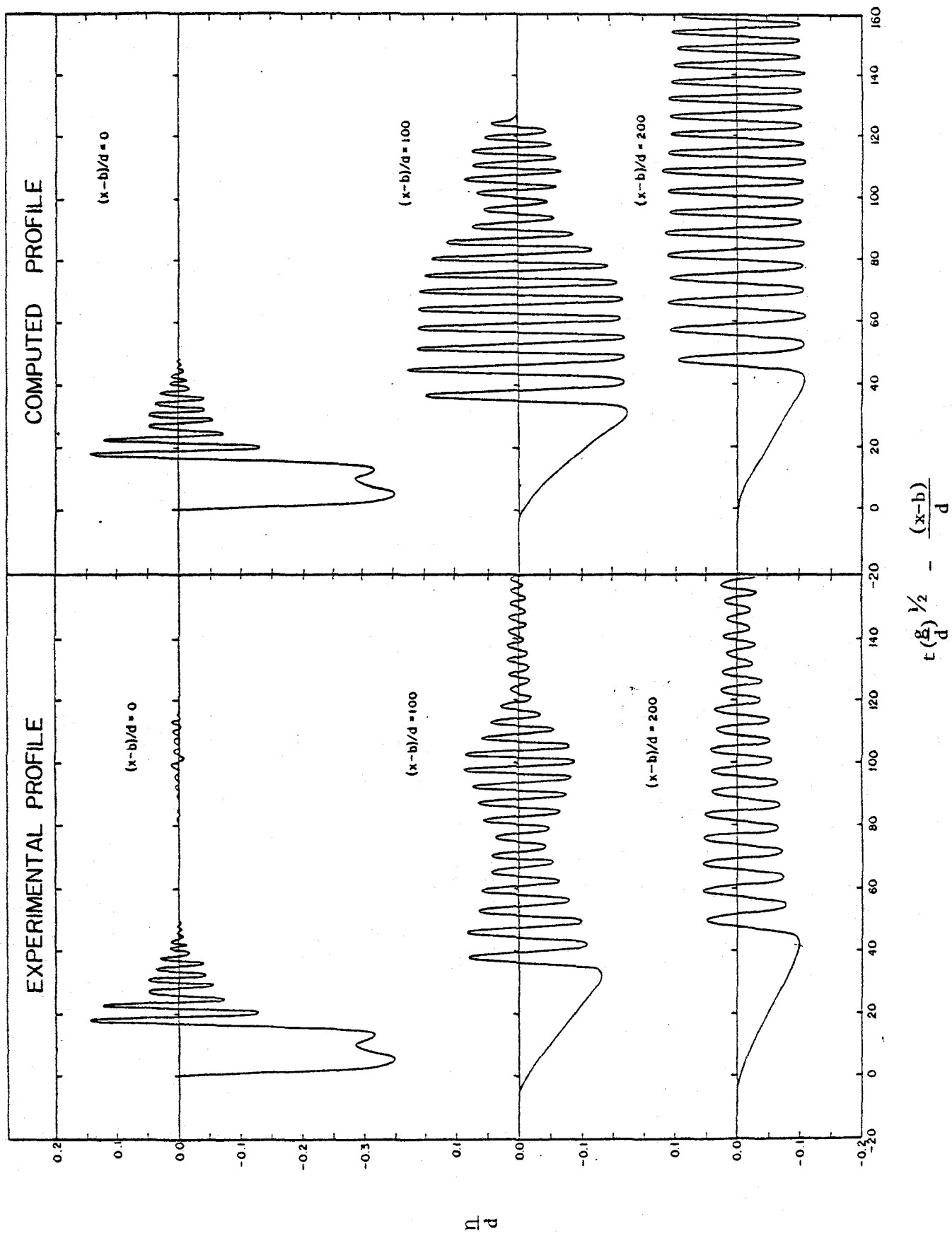


Fig. 9. Comparison of the present numerical wave profiles (for  $\nu = 1 \times 10^{-5}$  ft<sup>2</sup>/sec.) with the experimental wave profiles of Hammack & Segur (1975) at different stations (water depth  $d = 10$  cm.)

APPENDIX: COMPUTATIONAL ASPECTS

In the theoretical analysis there involves a characteristic horizontal length  $L$ . For solitary waves we adopt the distance between the two points of a solitary wave where  $\eta^*/\eta_0^* = 0.001$  to be the length " $L$ "; thus, for solitary waves  $L$  is defined as:

$$\frac{L}{d} = 10\sqrt{d/\eta_0^*} = \frac{10}{\sqrt{\epsilon}}$$

For the initial wave profiles presented in Figs. 4, 6, 8 and 9, the distance between the first two zero points in  $\eta^*$  is used as  $L$ : for example,  $L = 161$  cm. for the case of Fig. 6, and  $L = 170$  cm. for the case in Fig. 9.

For the numerical calculation, Eq. 15 is written in a finite-difference approximation as follows:

$$\begin{aligned} & \frac{H_j^{m+1} - H_j^{m-1}}{2\Delta\tau} + \left(\frac{3}{2}\right) \left(\frac{1}{3}\right) \left(\frac{1}{2\Delta\xi}\right) (H_{j+1}^m + H_j^m + H_{j-1}^m) (H_{j+1}^m - H_{j-1}^m) \\ & + \frac{\kappa}{6} \left(\frac{1}{2\Delta\xi^2}\right) (H_{j+2}^m - 2H_{j+1}^m + 2H_{j-1}^m - H_{j-2}^m) \\ & = \frac{a}{\Delta\xi^2} (-H_j^{m-1} + H_{j-1}^m + H_{j+1}^m - H_j^{m+1}) - \frac{\alpha}{3} (H_{j+1}^m + H_j^m + H_{j-1}^m) \end{aligned}$$

where  $H_j^m$  is  $\eta(m\Delta\tau, j\Delta\xi)$ . As mentioned in the main text, the difference in the computed profiles is extremely small whether we set  $a = 0$  or " $a$ " equals to the computed value based on Eq. 15. The stability condition by Vliegenthart (1971),  $\frac{\Delta\tau}{\Delta\xi} \left[ \frac{3}{2} |\eta| + \frac{4\kappa}{6\Delta\xi^2} \right]$ , is followed for all the calculations. In calculating the profiles used in Figs. 2 to 7, 240 points in  $\xi$  coordinate is used with  $\Delta\xi = 0.1$ . When calculating the profiles for Fig. 8, 340 points in  $\xi$  is used (with  $\Delta\xi = 0.1$ ) to account for the longer wave train developed in the tail region. However, for

the profile in Fig. 9, an even larger number of grid points is used. For Fig. 9, 640 points in  $\xi$  (with  $\Delta\xi = 0.1$ ) are used for calculating the wave profile at  $x = 100d$  from the initial station. Then the profile so obtained is used as an initial condition to find the wave profile at  $x = 200d$ . In this stage of computation, 940 points in  $\xi$  (with  $\Delta\xi = 0.1$ ) have been used. All computations are done with  $\Delta\tau = 0.00025$ .

The numerical computations are done by using IBM 370/178 computer. As an indication of the computation time involved, to obtain the profiles presented in Fig. 6, it requires 170 seconds of computation time.

## REFERENCES

- French, J.A. 1969. Wave uplift pressures on horizontal platforms. W. M. Keck Lab. of Hydraulics and Water Resources, Calif. Inst. Tech. Report KH-R-19.
- Gardner, C.S., Greene, J.M., Kruskal, M.D. & Miura, R.M., 1967. Method for solving the Korteweg-de Vries equation, Physics Review Letters, 19, 1095-1097.
- Hammack, J.L., 1973. A note on tsunamis: their generation and propagation in an ocean of uniform depth. J. Fluid Mechanics, 60, 769-799.
- Hammack, J.L. & Segur, H., 1974. The KdV equation and water waves. J. Fluid Mech., 65, 289-314.
- Hammack J.L. and Segur, H. 1975. Water wave propagation - Linear and non-linear theories, Proceedings Civil Engineering in the Oceans, III, p. 1247-1265.
- Ippen, A. T. 1966. Estuary and coastline hydrodynamics. McGraw-Hill, p. 125-127.
- Ippen, A.T., Kulin, G. & Raza, M.A. 1955. Damping characteristics of the solitary waves, Hydrodynamics Lab. M.I.T. Tech. Report No. 16.
- Ippen, A.T. & Mitchell, M.M. 1957. The damping of the solitary wave from boundary shear measurements, Hydrodynamics Lab. M.I.T. Report No. 23.
- Johnson, R. S. 1972. Some numerical solutions of a variable coefficient KdV equation. J. Fluid Mech., 54, 81-91.
- Johnson, R. S. 1973. On the development of a solitary wave moving over an uneven bottom. Proc. Camb. Phil. Soc., 73, 183-203.
- Keulegan, G. H. 1948. Gradual damping of solitary waves, Natl. Bur. Standard, 40, 487-498.
- Miles, J.W. 1976. Korteweg-de Vries equation modified by viscosity. The Physics of Fluids, Vol. 19, No. 7, July 1976, p. 1063.
- Ostrovskiy, L.A. & Pelinovskiy, Y. N. 1974. Nonlinear waves in inhomogeneous dissipative media. Fluid Mech. Soviet Research, 3, No. 6, 111-117.
- Ott, E & Sudan, R. N. 1970. Damping of solitary waves, The Physics of Fluids, Vol. 13, No. 6, p. 1432-1434.
- Shuto, N. 1976, Transformation of nonlinear waves, Abstracts of paper at Fifteenth Conference on Coastal Engineering, July 11 - 17, 1976, Honolulu, Hawaii, 692-694.

- Segur, H. 1973. The Korteweg-de Vries equation and water waves, Part 1. Solutions of the equation. J. of Fluid Mechanics, 59, p. 731 - 736.
- Van Dorn, W. G. 1966. Boundary dissipation of oscillatory waves. J. of Fluid Mechanics 24, 769 - 779.
- Vliegenthart, A.C. 1971. On finite-difference methods for the KdV equation. J. Eng. Math. 5, 137-155.
- Webster, A. G. 1955. Partial differential equations of mathematical physics, Dover Publications, Inc.
- Whitham, G. B. 1974. Linear and nonlinear waves. Wiley Interscience.
- Zabusky, N. J. & Galvin, C. J. 1971. Shallow-water waves, KdV equation and solitons. J. Fluid Mech., 47, 811-824.

#### 4.1. Introduction.

A class of problems involving the propagation of water waves in a fluid of variable depth is one in which the depth is constant except for variations over a finite interval. Interest in these problems is largely due to the phenomena associated with the passage of waves over submarine trenches in the ocean and wave propagation across navigational channels, where changes in water depth are commonly the case. A general analysis of wave propagation over variable depth geometries is given by Kreisel (1949). Kreisel's approach involves mapping the domain of the fluid into a rectangular strip, whereby the problem is reduced to a linear integral equation which can be solved by iteration for suitable geometries. An important aspect of problems involving changes in water depth is that of matching the solution along a geometrical boundary that separates the regions of different depths. Such an approach is found in the work of Bartholomeusz (1958) and Miles (1967). It has also been found (Newman, 1965) that for wave propagation over submarine obstacles there exists an infinite set of wavelengths such that the incident wave is totally transmitted.

This present study is restricted to the two-dimensional motion of linear periodic water waves over a rectangular submarine trench where the water depth before and after the trench is constant. The constant depth region and the trench region are separated geometrically and the velocity potential in each region is then found due to an unknown velocity distribution along the trench-constant depth boundary. This unknown

velocity distribution and consequently, the final solution can be obtained once an incident wave is specified and that the solutions in each region are matched along the common boundary. A major advantage inherent in this approach is that the solution for a trench of arbitrary shape can also be easily obtained.

#### 4.2. The boundary-value problem.

Let  $(x,y)$  constitute a Cartesian coordinate system with  $y = 0$  coinciding with the impermeable boundary of the constant depth region as shown in the definition sketch in Figure 1. Assuming a steady-state solution for the velocity potential in the form of

$$\Phi(x,y;t) = \phi(x,y)e^{-i\sigma t} \quad (2.1)$$

the potential function  $\phi(x,y)$  must satisfy Laplace's equation throughout the fluid domain and the following boundary conditions:

$$\begin{aligned} \frac{\partial \phi}{\partial y} &= \frac{\sigma^2}{g} \phi & \text{on } y = h, \quad -\infty < x < \infty \\ \frac{\partial \phi}{\partial y} &= 0 & \text{on } y = 0, \quad x < 0 \\ \frac{\partial \phi}{\partial y} &= 0 & \text{on } y = 0, \quad x > \lambda \\ \frac{\partial \phi}{\partial y} &= 0 & \text{on } y = -d, \quad 0 < x < \lambda \\ \frac{\partial \phi}{\partial x} &= 0 & \text{on } x = 0, \quad -d \leq y \leq 0 \\ \frac{\partial \phi}{\partial x} &= 0 & \text{on } x = \lambda, \quad -d \leq y \leq 0 \end{aligned} \quad (2.2)$$

In equation (2.1),  $\sigma$  represents the circular frequency,  $2\pi/\text{wave period}$ ;  $i$  is the complex number  $\sqrt{-1}$ .

In order to solve for  $\phi(x,y)$  in an efficient manner, the fluid domain is divided into two regions, Region I and Region II, (as shown also in Figure 1) by the common boundary  $\Gamma$  which is defined by

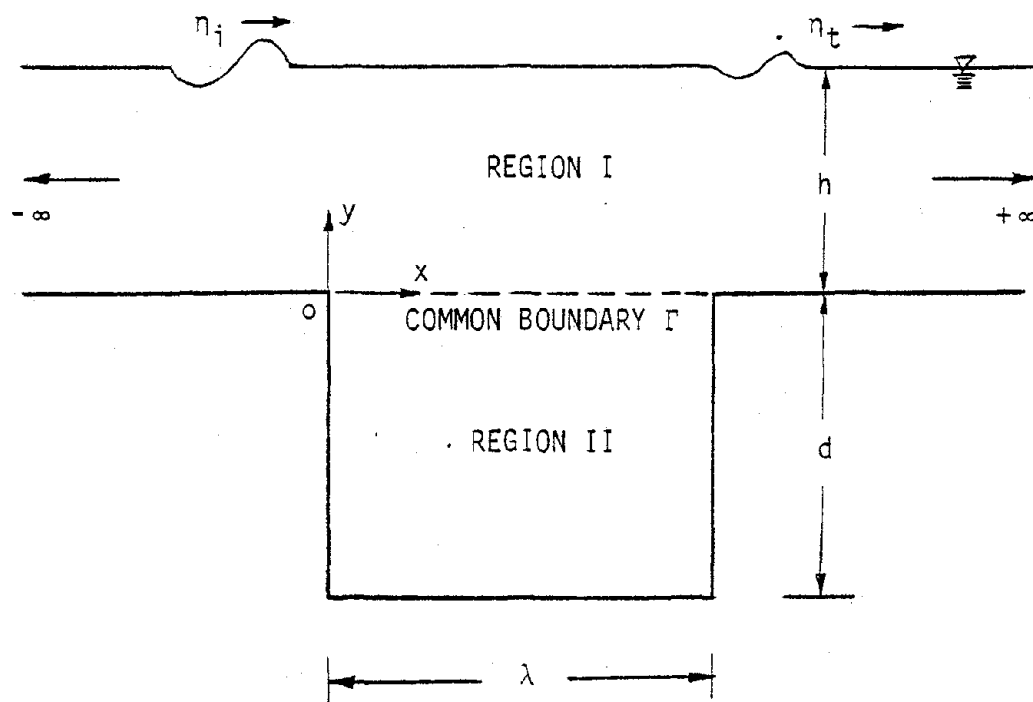


Figure 1 Definition sketch of the trench with regions of consideration.

$$y = 0 \quad , \quad 0 \leq x \leq \lambda .$$

Thus Region I is defined by

$$0 \leq y \leq h \quad , \quad -\infty < x < \infty$$

and Region II is defined by

$$-d \leq y \leq 0 \quad , \quad 0 \leq x \leq \lambda .$$

The strategy used herein is to solve for  $\phi(x,y)$  in each respective region in terms of the unknown  $\partial\phi/\partial y$  along the common boundary  $\Gamma$ .

Thus, by matching the solutions in each region at  $\Gamma$ , one is able to obtain the final solution.

### 4. 3. Region I solution.

Assuming a solution for the velocity potential in Region I to have the form

$$\Phi_I(x,y; t) = \phi_I(x,y) e^{-i\sigma t} ,$$

the potential  $\phi_I$  can be seen to satisfy Laplace's equation subject to the following boundary conditions:

$$\frac{\partial \phi_I}{\partial y} = \frac{\sigma^2}{g} \phi_I \quad \text{on } y = h , \quad -\infty < x < +\infty \quad (3.1)$$

$$\frac{\partial \phi_I}{\partial y} = g(x) \quad \text{on } y = 0 , \quad 0 < x < \lambda \quad (3.2)$$

$$\frac{\partial \phi_I}{\partial y} = 0 \quad \text{on } y = 0 , \quad x < 0 \quad (3.3)$$

$$\frac{\partial \phi_I}{\partial y} = 0 \quad \text{on } y = 0 , \quad x > \lambda \quad (3.4)$$

where  $g(x)$  represents the unknown velocity distribution along the trench-constant depth boundary.

The solution for  $\phi_I$  is determined using the Fourier Transform defined by

$$\mathcal{F}(f(x)) = \tilde{f}(k) = \int_{-\infty}^{\infty} f(x) e^{-ikx} dx$$

with the inverse transformation defined by

$$\mathcal{F}^{-1}(\tilde{f}(k)) = f(x) = \frac{1}{2\pi} \int_{-\infty}^{\infty} \tilde{f}(k) e^{ikx} dk .$$

The transformation of the governing equation subject to the transformed equations (3.1) - (3.4) and the subsequent inversion yields

$$\phi_I(x,y) = \frac{1}{2\pi} \int_{-\infty}^{\infty} \frac{\tilde{g}(k)}{k} \left[ \frac{(k + \sigma^2/g) e^{k(y-h)} + (k - \sigma^2/g) e^{k(h-y)}}{(k + \sigma^2/g) e^{-kh} - (k - \sigma^2/g) e^{kh}} \right] e^{ikx} dk \quad (3.5)$$

The still unknown function  $g(x)$  can be represented approximately by

$$g(x) \cong \sum_{j=1}^N Q_j [H(x-x_{j-1}) - H(x-x_j)] \quad (3.6)$$

where the interval  $0 < x < \lambda$  has been partitioned into  $N$  segments of equal length,  $Q_j$  is the average value of  $g(x)$  in the  $j^{\text{th}}$  subinterval, ( $j = 1, 2, \dots, N$ ), and  $H(x - \xi)$  is a Heavyside function defined by

$$H(x-\xi) = \begin{cases} 0 & x < \xi \\ 1 & x > \xi \end{cases}$$

A Fourier transform of (3.6) and substitution into (3.5) yields

$$\phi_I(x,y) = \frac{1}{2\pi i} \sum_{j=1}^N Q_j [I_{j-1} - I_j]$$

where

$$I_j = \int_{-\infty}^{\infty} \frac{e^{ik(x-x_j)}}{k^2} \left[ \frac{(k + \sigma^2/g) e^{k(y-h)} + (k - \sigma^2/g) e^{k(h-y)}}{(k + \sigma^2/g) e^{-kh} - (k - \sigma^2/g) e^{kh}} \right] dk$$

To compute the integral defined by  $I_j$ , the calculus of residues has been used; the integral  $I_j$  has simple poles at  $0, \pm k_r$  and  $\pm ik_n$  ( $n = 1, 2, \dots$ )

where  $k_r$  and  $k_n$  are defined by the following relationships:

$$\frac{\sigma^2}{g} = k_r \tanh(k_r \cdot h)$$

and

$$\frac{\sigma^2}{g} = -k_n \tan(k_n \cdot h)$$

In order to obtain an outgoing wave solution from the trench, we specify our inversion path to lie above the pole at  $-k_r$  and below the pole at  $+k_r$ . For such a path, the solution for  $\phi_I$  can be described as follows:

(1) If  $x > x_j$  for all  $j$ ,

$$\begin{aligned} \phi_I(x, y) = & \sum_{j=1}^N Q_j \left\{ \frac{\left[ e^{ik_r(x-x_j)} - e^{ik_r(x-x_{j-1})} \right]}{k_r^2} \cdot S_r(k_r, y) \right. \\ & \left. + \sum_{n=1}^{\infty} \frac{\left[ e^{-k_n(x-x_{j-1})} - e^{-k_n(x-x_j)} \right]}{k_n^2} \cdot S_n(k_n, y) \right\} \end{aligned} \quad (3.7)$$

(2) If  $x < x_j$  for all  $j$ ,

$$\begin{aligned} \phi_I(x, y) = & \sum_{j=1}^N Q_j \left\{ \frac{\left[ e^{-ik_r(x-x_{j-1})} - e^{-ik_r(x-x_j)} \right]}{k_r^2} \cdot S_r(k_r, y) \right. \\ & \left. + \sum_{n=1}^{\infty} \frac{\left[ e^{k_n(x-x_j)} - e^{k_n(x-x_{j-1})} \right]}{k_n^2} \cdot S_n(k_n, y) \right\} \end{aligned} \quad (3.8)$$

(3) If  $x > x_{j-1}$  and  $x < x_j$  for some  $j$ ,

$$\begin{aligned} \phi_I(x, y) = & \sum_{j=1}^{j-1} Q_j \left\{ \frac{\left[ e^{ik_r(x-x_j)} - e^{ik_r(x-x_{j-1})} \right]}{k_r^2} \cdot S_r(k_r, y) \right. \\ & \left. + \sum_{n=1}^{\infty} \frac{\left[ e^{-k_n(x-x_{j-1})} - e^{-k_n(x-x_j)} \right]}{k_n^2} \cdot S_n(k_n, y) \right\} \\ & + Q_j \left[ \frac{1 + \sigma^2/g (y-h)}{\sigma^2/g} - \frac{\left[ e^{ik_r(x-x_{j-1})} + e^{-ik_r(x-x_j)} \right]}{k_r^2} \right] \cdot S_r(k_r, y) \end{aligned}$$

$$\begin{aligned}
& + \sum_{n=1}^{\infty} \left[ \frac{e^{-k_n(x-x_{j-1})} + e^{-ik_r(x-x_j)}}{k_n^2} \cdot S_n(k_n, y) \right] \\
& + \sum_{j+1}^N Q_j \left\{ \frac{e^{-ik_r(x-x_{j-1})} - e^{-ik_r(x-x_j)}}{k_r^2} \cdot S_r(k_r, y) \right. \\
& \left. + \sum_{n=1}^{\infty} \frac{e^{k_n(x-x_j)} - e^{k_n(x-x_{j-1})}}{k_n^2} \cdot S_n(k_n, y) \right\} \quad (3.9)
\end{aligned}$$

In equations (3.7) - (3.9) the functions  $S_r$  and  $S_n$  are defined by

$$S_r(k_r, y) = \frac{k_r \cosh[k_r(y-h)] + \sigma^2/g \sinh[k_r(y-h)]}{k_r h \operatorname{sech} k_r h + \sinh k_r h}$$

and

$$S_n(k_n, y) = \frac{k_n \cos[k_n(y-h)] + \sigma^2/g \sin[k_n(y-h)]}{k_n h \sec k_n h + \sin k_n h}$$

It is easily verified that the solution for  $\phi_I$  given by (3.7) - (3.9) satisfies Laplace's equation in Region I and the associated boundary conditions (3.1) - (3.4).

#### 4. 4. Region II solution.

Again, the solution for the velocity potential in Region II has the steady-state form

$$\Phi_{II}(x,y;t) = \phi_{II}(x,y) e^{-i\sigma t}$$

and the potential  $\phi_{II}$  must satisfy Laplace's equation subject to the following boundary conditions:

$$\frac{\partial \phi_{II}}{\partial x} = 0 \quad \text{on } x = 0, \quad -d \leq y \leq 0 \quad (4.1)$$

$$\frac{\partial \phi_{II}}{\partial x} = 0 \quad \text{on } x = \lambda, \quad -d \leq y \leq 0 \quad (4.2)$$

$$\frac{\partial \phi_{II}}{\partial y} = 0 \quad \text{on } y = -d, \quad 0 \leq x \leq \lambda \quad (4.3)$$

$$\frac{\partial \phi_{II}}{\partial y} = g(x) \quad \text{on } y = 0, \quad 0 \leq x \leq \lambda \quad (4.4)$$

There exists a constraint on  $g(x)$ ; namely that due to the conservation of mass in Region II

$$\int_0^\lambda g(x) dx = 0 \quad (4.5)$$

Using the approximate representation for  $g(x)$ , Equation (4.5) and (3.6) can be combined to give

$$\sum_{j=1}^N Q_j = 0, \quad \text{a condition which necessarily must be} \quad (4.6)$$

also applied to Region I.

Via the technique of separation of variables, the solution for the potential  $\phi_{II}$  subject to the boundary conditions (4.1) - (4-4) is

$$\phi_{II}(x,y) = \alpha_0 + \sum_{n=1}^{\infty} \alpha_n \cos \frac{n\pi x}{\lambda} \cdot \cosh \frac{n\pi(y+d)}{\lambda} \quad (4.7)$$

where  $\alpha_0$  is an arbitrary constant, and  $\alpha_n (n \geq 1)$  is given by

$$\alpha_n = \frac{2}{n\pi \cdot \sinh \left( \frac{n\pi d}{\lambda} \right)} \cdot \int_0^{\lambda} g(x) \cdot \cos \frac{n\pi x}{\lambda} dx \quad (4.8)$$

4.5. Superposition and matching of solutions.

For a periodic incident wave travelling in the positive  $x$  direction in Region I, the velocity potential can be specified as

$$\Phi_{in}(x,y;t) = \phi_{in} \cdot e^{-i\sigma t} = \frac{ag}{i\sigma} \frac{\cosh k_r y}{\cosh k_r h} e^{i(k_r x - \sigma t)} \quad (5.1)$$

Defining  $\hat{x}_j$  ( $j = 1, 2, \dots, N$ ) as the midpoint of the  $j^{\text{th}}$  subinterval of  $\Gamma$ , we may in turn define the vector  $\{\phi_{in}\}_{N \times 1}$  by

$$\phi_{in}^{(j)} = \phi_{in}(\hat{x}_j, 0) = \frac{ag}{i\sigma} \operatorname{sech} k_r h e^{ik_r \hat{x}_j} \quad (5.2)$$

where  $\phi_{in}^{(j)}$  denotes the  $j^{\text{th}}$  member of the vector  $\{\phi_{in}\}$ . Similarly, a vector  $\{\phi_I\}$  can be defined by

$$\phi_I^{(j)} = \phi_I(\hat{x}_j, 0) \quad (5.3)$$

Using equation (3.9), it can be shown that  $\{\phi_I\} = [H] \{Q\}$ , where  $H$  is symmetric with the additional property that

$$H_{i+1,j+1} = H_{ij}, \quad (i, j = 1, 2, \dots, N-1)$$

and

$$Q^{(j)} = Q_j$$

Defining the column vector  $\{\phi_{II}\}$  by  $\phi_{II}^{(j)} = \phi_{II}(\hat{x}_j, 0)$ , equations (3.6) and (4.8) gives

$$\{\phi_{II}\} = \{\beta_0\} + [B] \cdot [M] \{Q\} \quad (5.4)$$

where  $\{\beta_0\}_{N \times 1}$  is a vector in which each member is (the same) arbitrary constant,  $[B]_{N \times P}$  is a matrix defined by

$$B_{np} = \cos \frac{p\pi\hat{x}_n}{\lambda} \cdot \coth \frac{p\pi d}{\lambda} \quad \left( \begin{array}{l} n = 1, \dots, N \\ p = 1, \dots, P \end{array} \right)$$

where  $P$  denotes an upper limit to the Fourier series representation of  $\phi_{II}(x,y)$ , and the matrix  $[M]_{P \times N}$  is given by

$$M_{pn} = \frac{4\lambda}{(p\pi)^2} \sin \frac{p\pi}{2N} \cdot \cos \frac{p\pi\hat{x}_n}{\lambda}$$

Due to the continuity of velocity potential along the common boundary  $\Gamma$  we have

$$\{\phi_{in}\} + \{\phi_I\} = \{\phi_{II}\} \quad (5.5)$$

Substituting equations (5.2) - (5.4) into (5.5) we obtain  $N$  equations with  $N + 1$  unknowns ( $Q_1, Q_2, \dots, Q_N$  and  $\beta_0$ ). However, equation (4.6) must again be implemented for Region I, providing us with an additional equation. This system of linear equations is then solved numerically for the vector  $\{Q\}$ . Thus, the originally unknown function  $g(x)$  introduced in equation (3.2) is now solved as a discrete function  $\{Q\}$

#### 4.6. Wave amplitude analysis.

Since the values of  $Q_j$  have been found, the velocity potential in the entire domain is completely solved. In particular, the values of  $\phi_I$  and  $\phi_{in}$  at the surface can now be computed using equations (3.7) - (3.9) and (5.1). The wave amplitude at the water surface is given by linear theory to be

$$a = \frac{1}{g} \left| \frac{\partial \phi_I}{\partial t} + \frac{\partial \phi_{in}}{\partial t} \right|_{@ y=h} = \frac{\sigma}{g} \left| \phi_I + \phi_{in} \right|_{@ y=h}$$

Consequently, the steady state amplitude of a surface wave at any value of  $x$  is determined.

#### 4. 7. Experimental equipment and procedure.

A series of laboratory experiments is conducted in a wave tank of 12 inches wide, 48 feet long and 18 inches deep. A paddle-type wave generator is placed at one end of the tank to generate the desired wave at a specified wave period. The wave period is controlled by a variable speed motor control. A wave filter is placed in front of the wave paddle while a wave absorber is located at the end of the wave tank. At the central section of the wave tank a special trench section is installed. The trench section extends  $26\frac{1}{2}$ " below the bottom of the wave tank to rest on the laboratory floor. The maximum trench length is 85 inches. Four different trench lengths can be obtained through the partitions installed, namely  $21\frac{1}{8}$ ",  $42\frac{3}{8}$ ",  $63\frac{5}{8}$ ", 85". The depth in the trench section can also be varied by placing a false bottom at various heights.

The wave amplitude is measured by means of resistant-type wave gauges. The wave records are recorded using a Hewlett Packard four channel oscillograph recorder.

Wave amplitudes were measured in the region 2 feet to 6 feet behind the trench section. Wave amplitude envelopes are obtained first without the effect of the trench (by covering the trench section completely) in order to determine the incident wave amplitude. The wave envelopes are then obtained with the trench at the desired length and depth at the same region behind the trench section in order to ascertain the wave amplitude after passing over the trench section.

#### 4.8. Presentation and Discussion of Results.

The effect of the trench on the propagation of waves can be demonstrated most easily by the transmission and reflection characteristics. Figure 2 shows the transmission coefficient,  $K_t$ , as a function of the relative wave length. The ordinate is the ratio of the transmitted wave amplitude divided by the incident wave amplitude, while the abscissa is the ratio of the water depth,  $h$ , in Region I divided by the incident wave length,  $L$ . The wave length  $L$  is computed from the dispersion relationship,  $L = (gT^2/2\pi) \tanh(2\pi h/L)$ , where  $T$  is the incident wave period. It is seen from Figure 2 that for  $h/L > 0.18$ , the incident waves are almost fully transmitted. At  $h/L = 0.09$ , the transmission coefficient is approximately 0.89. To understand the trench effect further, one can compute the value of  $\lambda/L$  at these critical points. At  $h/L = 0.18$ , it corresponds to  $\lambda/L = 0.95$  while at  $h/L = 0.09$ , it corresponds to  $\lambda/L = 0.475$ . It appears that for a relatively short trench length, the maximum reduction of transmitted wave occurs as  $\lambda/L$  approaches 0.5. As the wave period is decreased to where  $\lambda/L$  approaches 1, the effect on wave transmission due to the trench is negligible.

Figure 3 shows the reflection coefficient as a function of the relative wave length for the same range of  $h/L$  shown in Figure 2. The reflection coefficient,  $K_r$ , is defined as the reflected wave amplitude divided by incident wave amplitude. As expected, the maximum reflected wave occurs at  $h/L = 0.09$  where the transmitted wave is a minimum. As this is an inviscid theory, one can check the result

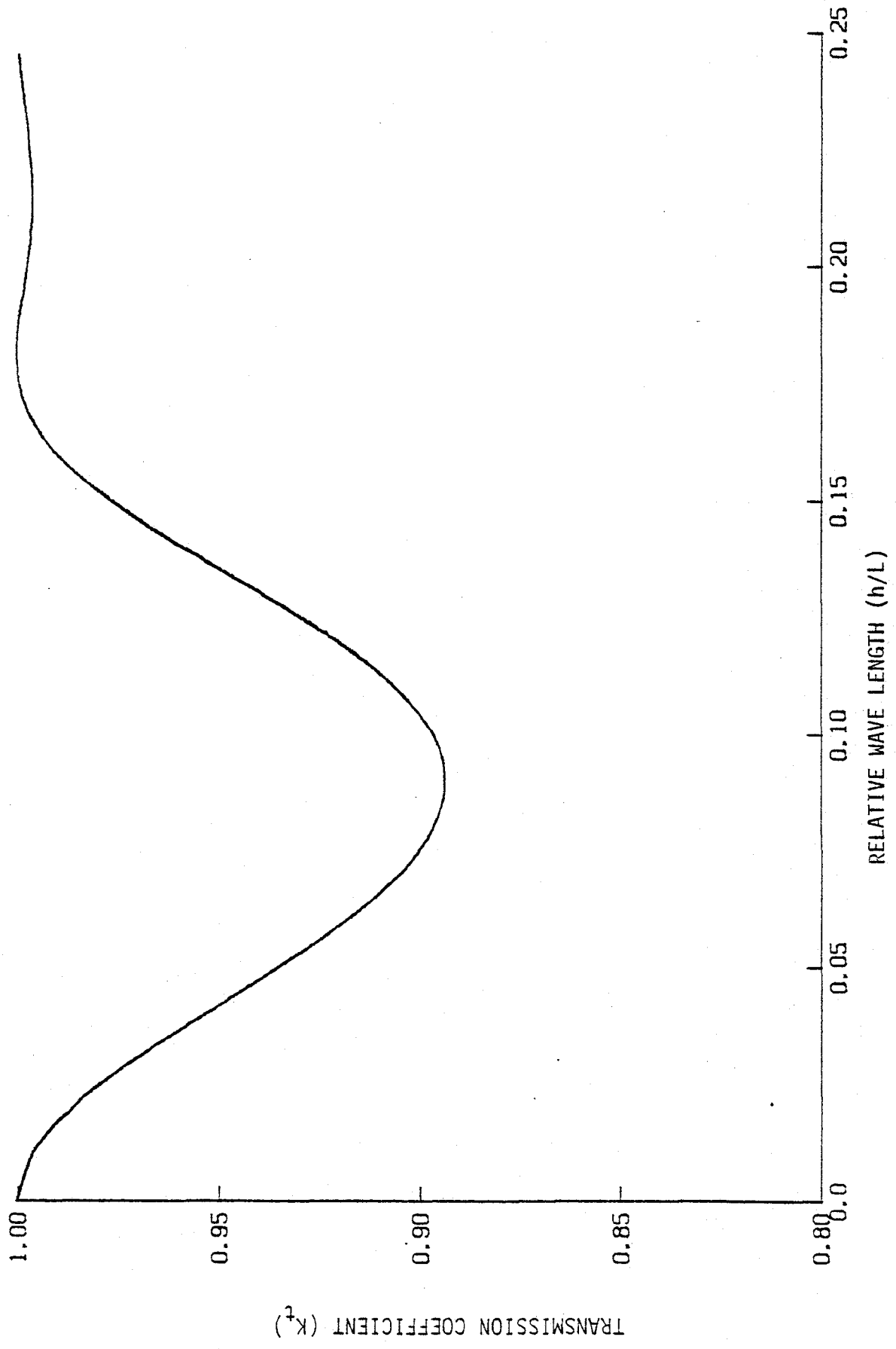


Figure 2 Transmission coefficient as a function of relative wave length ( $h = 4''$ ,  $d = 26\frac{1}{2}''$ ,  $\lambda = 21\frac{1}{8}''$ ).

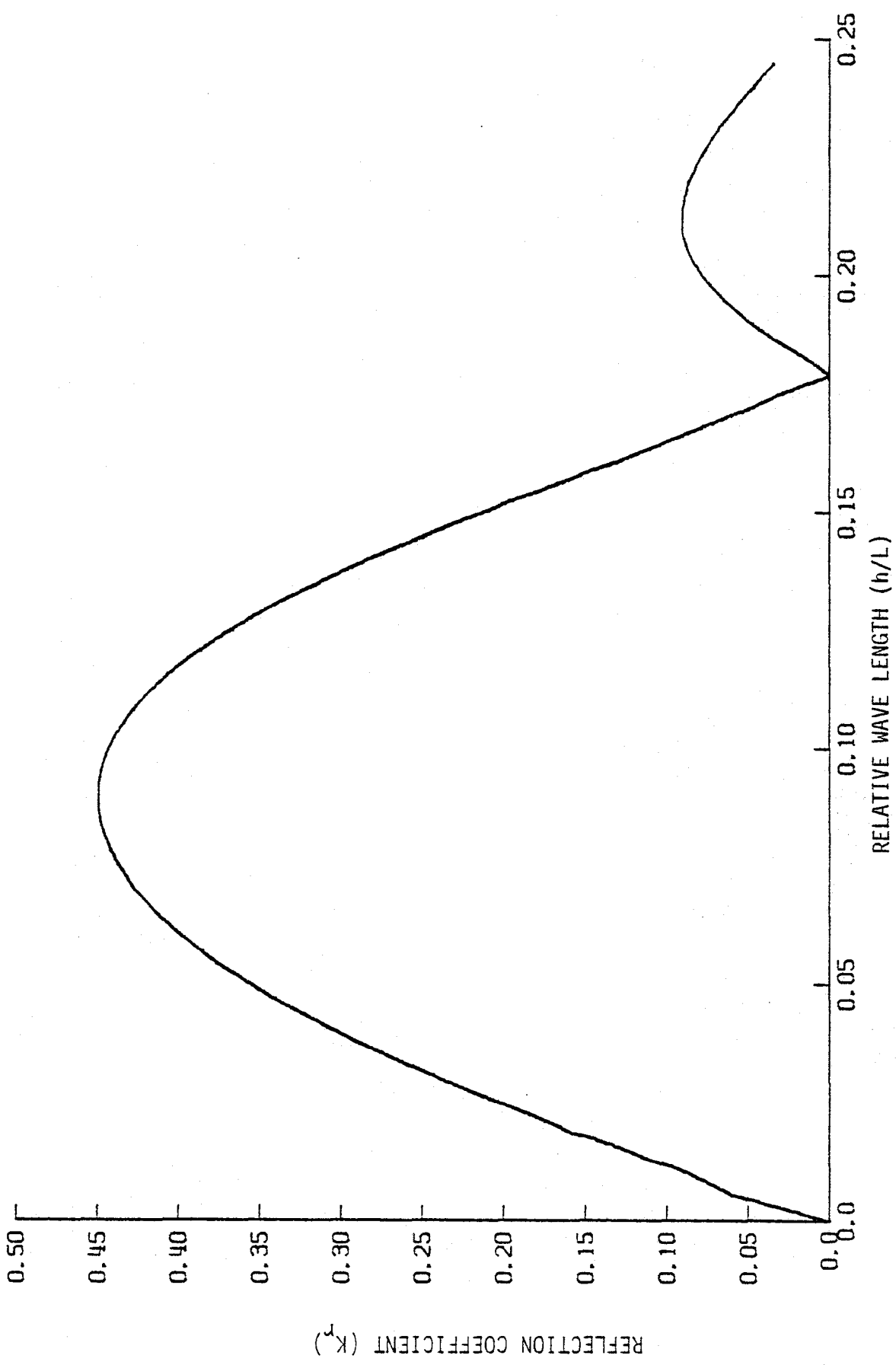


Figure 3 Reflection coefficient as a function of relative wave length ( $h = 4''$ ,  $d = 26\frac{1}{2}''$ ,  $\lambda = 21\frac{1}{8}''$ ).

to see whether  $K_r^2 + K_t^2 = 1$  can be satisfied (where  $K_r$  is the reflection coefficient,  $K_t$  the transmission coefficient). For the range of  $h/L$ , it is checked that such a relation holds true; thereby further increasing the validity of the theoretical result.

As the trench length increases, the effect of the trench on transmission and reflection characteristics becomes more interesting. This is shown in Figures 4 and 5. The trench length for this case is twice the length of that in Figures 2 and 3. It is seen for the range of  $h/L$  presented, there are four wave periods at which waves are fully transmitted ( $K_t = 1$ ,  $K_r = 0$ ). The reduction in transmission coefficient or increase in reflection coefficient is more pronounced at  $h/L = 0.056$ . Again, it was checked that the relationship  $K_r^2 + K_t^2 = 1$  held true. It is seen that the effect of the trench on transmission or reflection coefficients for higher values of  $h/L$  is decreasingly smaller. This is reasonable, because for higher values of  $h/L$ , the water depth is relatively deeper; therefore, an increase in water depth due to the trench will have a lesser impact on the transmitted wave.

In Figure 4 experimental data on the transmission coefficient has been included for comparison. It is seen that the experimental data in general confirms the trend predicted by the theoretical analysis. Since the effect of energy dissipation is not included in the theory, the data tends to have a lower value of  $K_t$ . Also apparent from the experimental data is that there exists an oscillation of data points about the theoretical curve. This could be due to

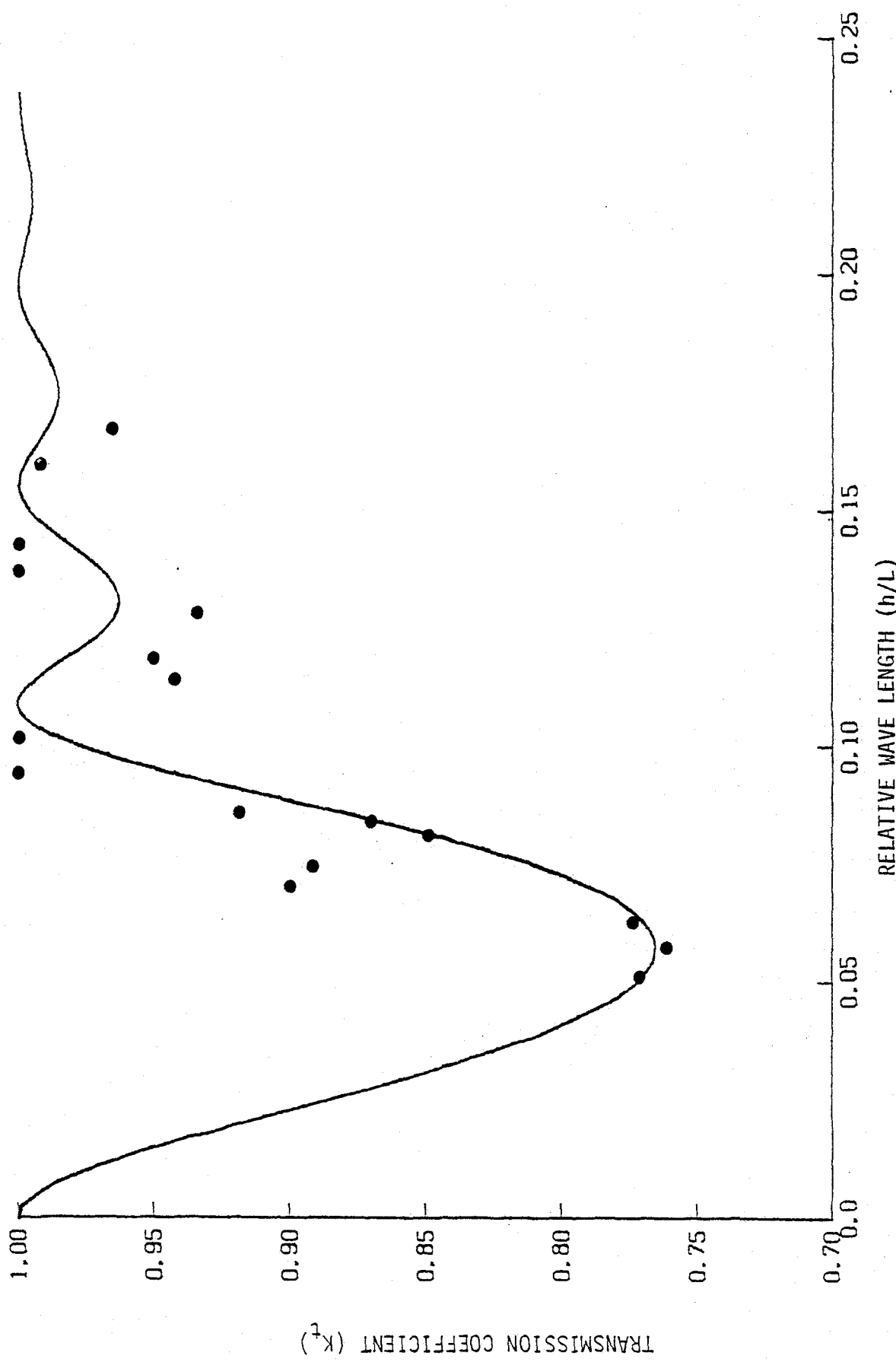


Figure 4 Transmission coefficient as a function of relative wave length ( $h = 4''$ ,  $d = 26\frac{1}{2}''$ ,  $\lambda = 42\frac{3}{8}''$ , ——— Theoretical results, ● Experimental data).

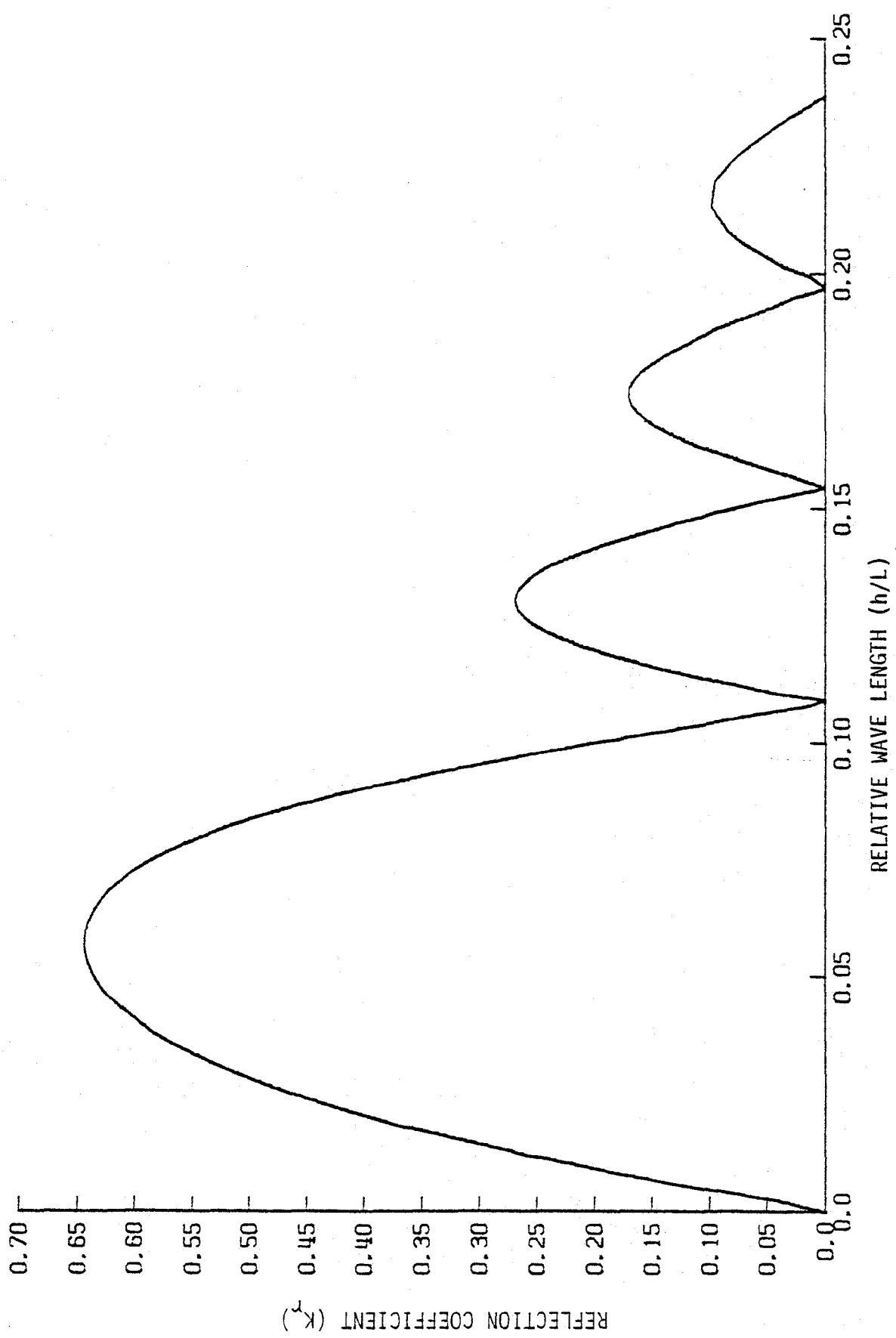


Figure 5 Reflection coefficient as a function of relative wave length  $(h = 4", d = 26\frac{1}{2}", \lambda = 42 \frac{3}{4})$

the effect of the finite length of the wave tank and that the wave absorbers placed at both ends of the wave tank cannot eliminate the wave reflection completely from the tank ends. Due to the limitation of the available experimental facilities, a substantially superior experimental verification is not achieved.

Results on wave transmission over a longer trench length is shown in Figure 6. The trench length for this case is three times that shown in Figure 2 with other dimensions held constant.

In the range of  $0 < h/L < 0.25$ , there are six different wave periods at which waves are fully transmitted. The results indicate that the trench does exert a greater influence on wave transmission characteristics in that the transmission coefficient at  $h/L = 0.042$  is only about 0.70. Experimental data are also included in Figure 6. It is seen that the experimental data in general tend to confirm the theoretical prediction. However, due to the unavoidable energy dissipation as well as reflection from both ends of the wave tank, the experimental data show considerable scattering as evident in the figure.

Figure 7 shows the wave transmission coefficient for a trench with a further increase in trench length. The number of wave periods at which waves are fully transmitted is now increased to nine for the same range of  $h/L$ . For each of the troughs in the response curve, the effect of the trench is further dramatized. For example, at the first trough ( $h/L = 0.034$ ), the transmission coefficient is reduced to 0.68, while at the second trough ( $h/L = 0.081$ ), the transmission coeffi-

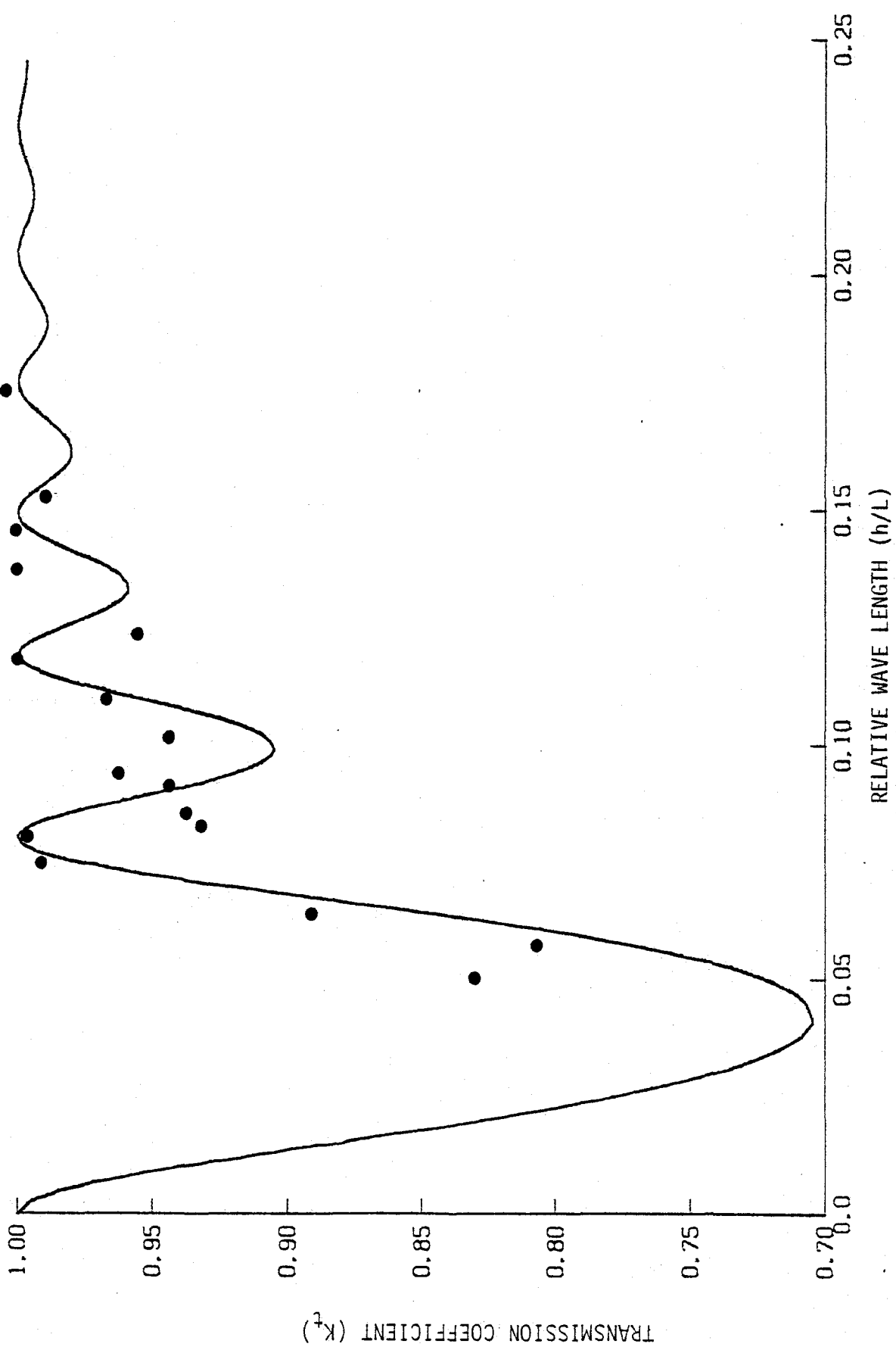


Figure 6 Transmission coefficient as a function of relative wave length ( $h = 4''$ ,  $d = 26\frac{1}{2}''$ ,  $\lambda = 63\frac{5}{8}''$ , ——— Theoretical results, ● Experimental results).

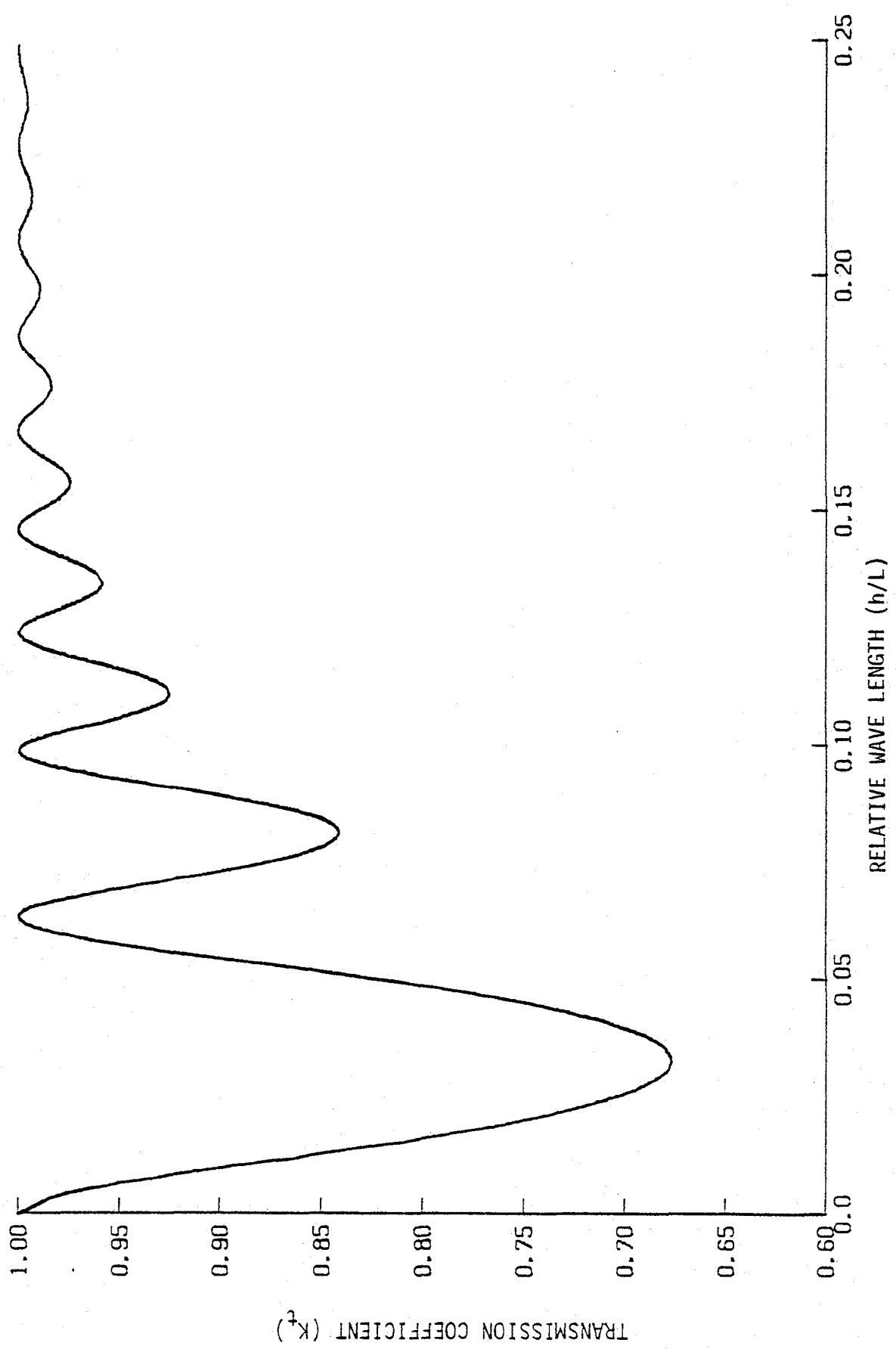


Figure 7 Transmission coefficient as a function of relative wave length ( $h = 4''$ ,  $d = 26\frac{1}{2}''$ ,  $\lambda = 85''$ ).

cient is about 0.84. These are clearly smaller values than those shown in Figure 6.

To show the effect of the water depth in the trench, the case for Figure 6 is changed to  $d = 1\frac{3}{4}$  inches (one-half of that presented in Figure 6). A curve showing the transmission coefficient is presented in Figure 8. As can be expected, the values of  $h/L$  corresponding to peaks and troughs in the response curve are slightly different. There is an increase in the wave transmission for the first trough while for the second trough the wave transmission is somewhat decreased. This is reasonable, because for a decrease in the value of  $d$ , the trench would not be so deep as to fall in the deep water wave range completely.

Figure 9 shows the results when the water depth in Region I is increased from 4 inches to 6 inches with other dimensions the same as that used in Figure 8. Again, it can be expected that the effect of the trench is somewhat lessened.

All the theoretical results presented so far are computed when the trench length is divided into 30 equal segments. Identical results have been obtained when the trench is divided into 50 segments. Of course, if the trench is very long, one should increase the number of segments in the trench mouth.

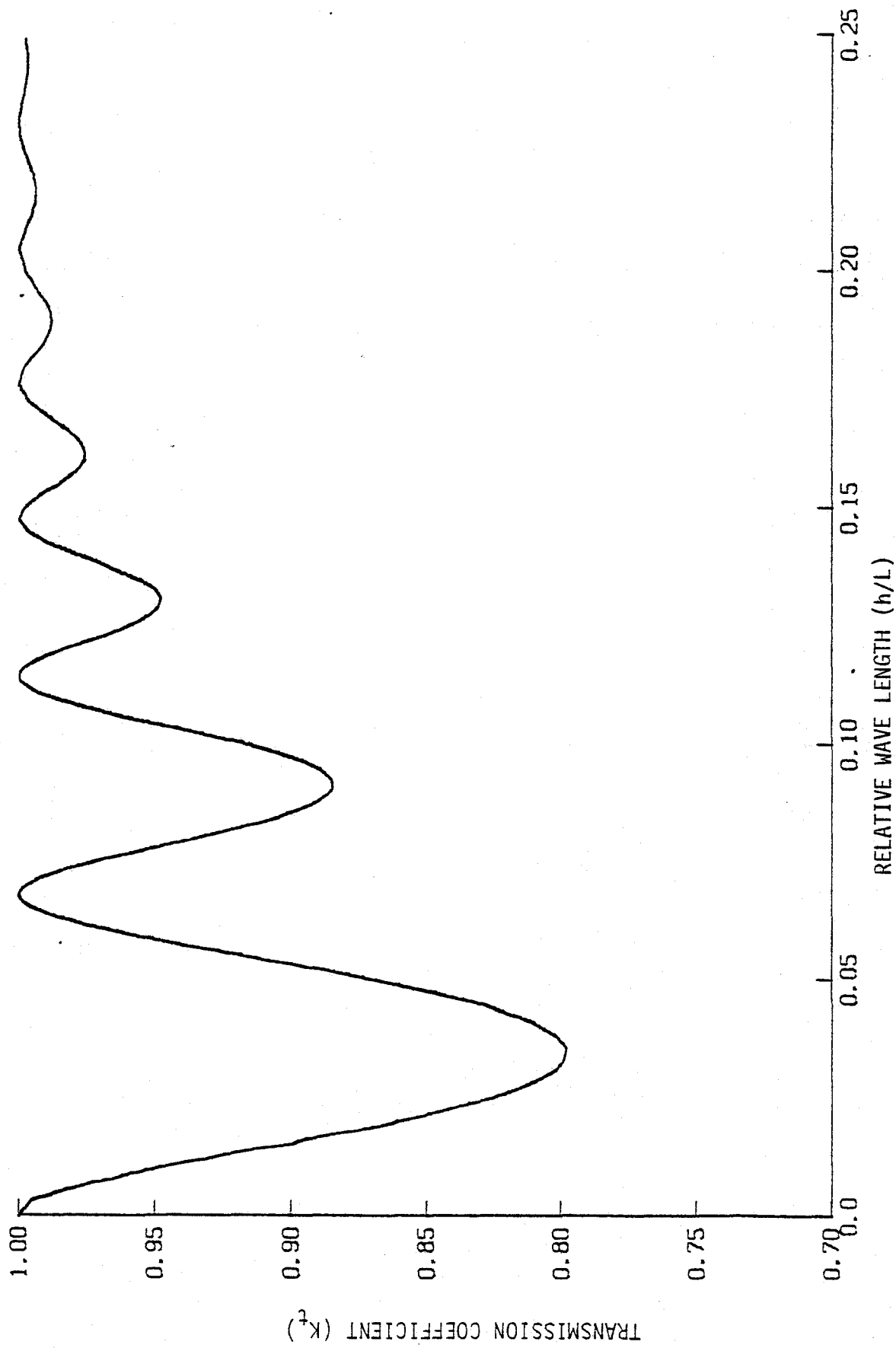


Figure 8 Transmission coefficient as a function of relative wave length ( $h = 4''$ ,  $d = 13\frac{1}{4}''$ ,

$\lambda = 63 \frac{5}{8}''$ ).

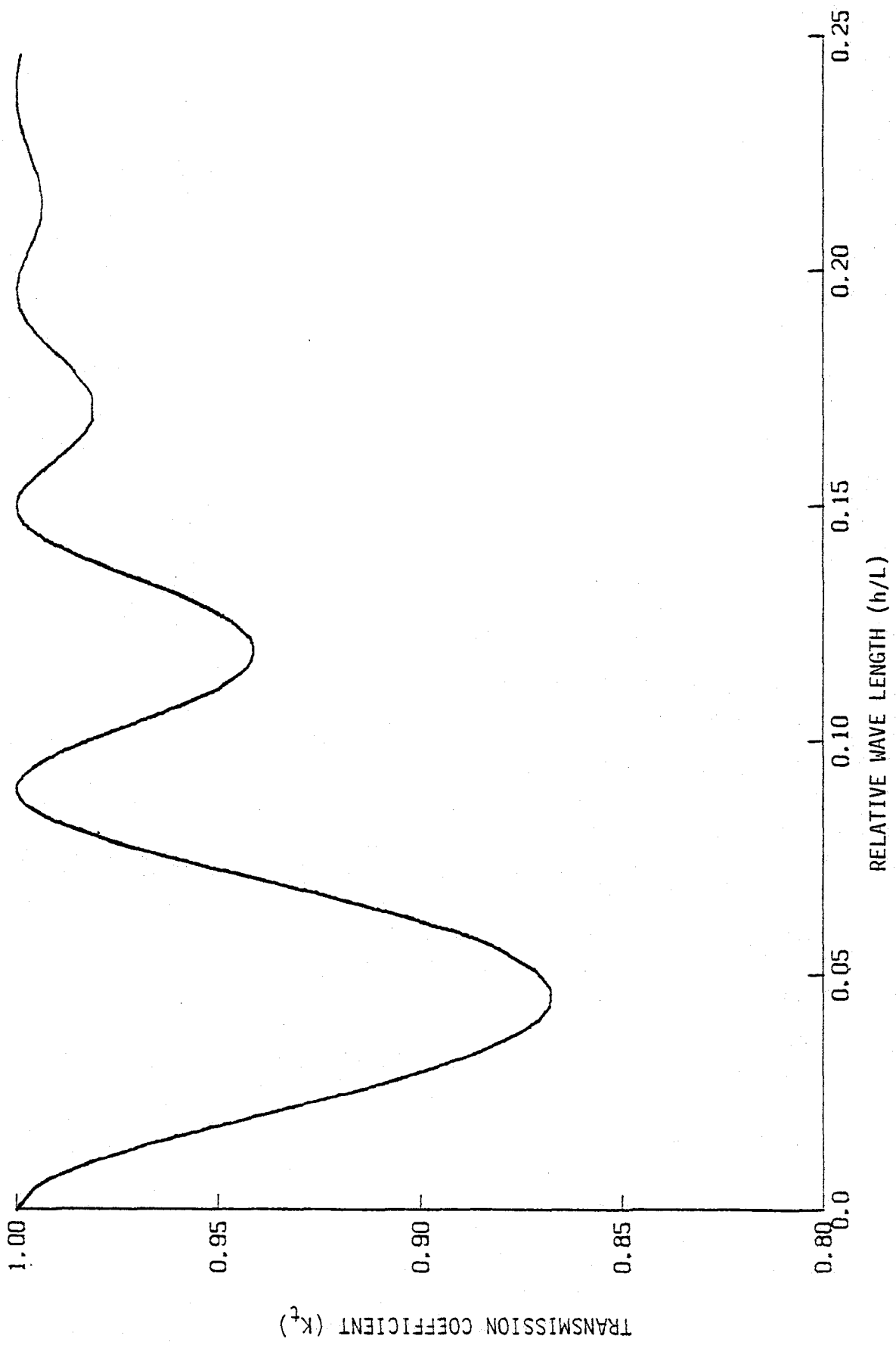


Figure 9 Transmission coefficient as a function of relative wave length ( $h = 6''$ ,  $d = 13\frac{3}{4}''$ ,  $\lambda = 63\frac{5}{8}''$ ).

#### 4.9. Concluding Remarks.

The method used for analyzing the effect of a rectangular trench on the propagation of periodic incident waves has been shown to be quite effective. From the results on wave transmission and reflection, it is seen that there exists an infinite number of wave periods at which waves are fully transmitted. The effect of the trench on wave transmission (or reflection) is progressively smaller for higher wave frequencies (the larger values of  $h/L$ ).

One advantage of the method presented here is that for a trench of arbitrary shape the solution in Region I need not be changed. Thus, any convenient method which can be used for Region II can be matched to obtain the final solution. This is being done in a subsequent study by the authors.

00

List of References

1. Bartholomeusz, E.F., "The Reflection of Long Waves at a Step," Proc. Camb. Phil. Soc., Vol. 54, 1958, p. 106.
2. Kreisel, H., "Surface Waves," Quarterly Applied Mathematics, Vol. 7, 1949, p. 21.
3. Miles, J.W., "Surface-Wave Scattering Matrix for a Shelf," Journal of Fluid Mechanics, Vol. 28, 1967, p. 755.
4. Newman, J.N., "Propagation of Water Waves Past Long Two-dimensional Obstacles," Journal of Fluid Mechanics, Vol. 23, 1965, p.23.
5. Newman, J.N., "Propagation of Water Waves over an Infinite Step," Journal of Fluid Mechanics, Vol. 23, 1965, p. 399.